

This document is confidential and is proprietary to the American Chemical Society and its authors. Do not copy or disclose without written permission. If you have received this item in error, notify the sender and delete all copies.

Exploring “triazole-thiourea” based Ligands for the Self-assembly of Photoluminescent Hg(II) Coordination Compounds

Journal:	<i>Crystal Growth & Design</i>
Manuscript ID	cg-2021-003522.R2
Manuscript Type:	Article
Date Submitted by the Author:	n/a
Complete List of Authors:	<p>Benaissa, Houria; Universite catholique de Louvain, Institute of Condensed Matter and Nanosciences Adarsh, Nayarassery N.; Gandhiji University Robeyns, Koen; Universite catholique de Louvain, Institute of Condensed Matter and Nanosciences (IMCN) Zakrzewski, Jakub; Jagiellonian University Chorazy, Szymon; Jagiellonian University, Faculty of Chemistry Hooper, James; Jagiellonian University, Department of Theoretical Chemistry Sagan, Filip; Jagiellonian University, Dept. of Theoretical Chemistry, Faculty of Chemistry Mitoraj, Mariusz; Uniwersytet Jagiellonski w Krakowie, Department of Theoretical Chemistry, Faculty of Chemistry Wolff, Dr. Mariusz; University of Linz, Institute of Inorganic Chemistry RADI, Smaail; Université Mohammed Premier Oujda Faculté des Sciences, Chemistry Garcia, Yann; Universite catholique de Louvain, Institute of Condensed Matter and Nanosciences</p>

SCHOLARONE™
Manuscripts

Exploring “triazole-thiourea” based Ligands for the Self-assembly of Photoluminescent Hg(II) Coordination Compounds

Houria Benaissa,^a Nayarassery N. Adarsh,^b Koen Robeyns,^a Jakub J. Zakrzewski,^c Szymon Chorazy,^c James G. M. Hooper,^d Filip Sagan,^d Mariusz P. Mitoraj,^d Mariusz Wolff,^{a,e} Smaail Radi,^f Yann Garcia^{a,*}

^aInstitute of Condensed Matter and Nanosciences, Molecular Chemistry, Materials and Catalysis (IMCN/MOST), Université catholique de Louvain, Place Louis Pasteur 1, 1348 Louvain-la-Neuve, Belgium. E-mail: yann.garcia@uclouvain.be

^bSchool of Chemical Sciences, Mahatma Gandhi University, Kottayam, 686560, Kerala, India.

^cInorganic Molecular Materials Group, Faculty of Chemistry, Jagiellonian University, Gronostajowa 2, 30-387 Krakow, Poland.

^dDepartment of Theoretical Chemistry, Faculty of Chemistry, Jagiellonian University, R. Ingardena 3, 30Fig-060 Krakow, Poland.

^eJohannes Kepler University Linz, Institute of Inorganic Chemistry, Altenbergerstraße 69, 4040 Linz, Austria

^fLCAE, Department of Chemistry, Faculty of Sciences, University Mohamed I, BP 524, 60 000 Oujda, Morocco.

ABSTRACT: This study represents the first explorative investigation on the supramolecular structural diversity in Hg(II) coordination chemistry with triazole-thiourea ligands leading to a variety of mononuclear, binuclear and coordination polymers: $\{[\text{Hg}(\mathbf{L1})_2(\mathbf{L1}^-)_2]\}$ (**1**), $\{[\text{Hg}_2(\mathbf{L1})_2(\mu_2\text{-I})_2]_2\} \cdot \text{DMSO}$ (**2**), $\{[\text{Hg}(\mathbf{L2})(\mu_2\text{-I})] \cdot \text{MeOH}\}_\infty$ (**3**), $\{[\text{Hg}_2(\mu\text{-L3}^-)_4]\}_\infty$ (**4**), $\{[\text{HgCl}(\mathbf{L4}^-)\mathbf{L4}] \cdot \text{MeOH}\}$ (**5**), $\{[\text{Hg}_2(\mathbf{L4})_2(\mu_2\text{-I})_2]_2\} \cdot 2\text{MeOH}$ (**6**), $\{[\text{Hg}_2(\mu_2\text{-L5}^-)_4]\}_\infty$ (**7**), $[\text{Hg}_2(\mu_2\text{-Cl})_2(\mathbf{L6}^-)_2(\mathbf{L6})_2]$ (**8**), $\{[\text{Hg}_2(\mu_2\text{-Br})_2(\mathbf{L6}^-)_2(\mathbf{L6})_2]\}$ (**9**) and $\{[\text{Hg}_2(\mu_2\text{-I})_2(\mathbf{L6}^-)_2(\mathbf{L6})_2]\}$ (**10**). A reaction mechanism was suggested for the unexpected ligand rearrangement occurring in $\{[\text{Hg}_2\text{I}_3(\mu_3\text{-L5}')]\}_\infty$ (**11**). The ligands were fully characterized including by X-ray crystallography and computational means. This includes six new triazole-thiourea based ligands namely 1-R-3-(4H-1,2,4-triazol-4-yl)thiourea (where R = methyl (**L1**), ethyl (**L2**), propyl (**L3**), isopropyl (**L4**) and its polymorph (**L4-poly**), allyl (**L5**), ethyl acetate (**L6**) and its solvate (**L6_MeOH**). Under UV light excitation, **7**, **10** and **11** exhibit visible photoluminescence of wide origin, ranging from ligand-centered (LC) fluorescence combined with organic-ligand-to-metal charge transfer (LMCT) emissive states in **7** and **10**, up to halide-to-metal charge transfer (XMCT) combined with halide-to-ligand

1
2
3 charge transfer (XLCT) emissive states in **11**. The variable emission mechanisms in
4 the obtained coordination polymers were elucidated by experimental proofs
5 confronted with theoretical calculations of the electronic densities of states, proving
6 that Hg(II) halide coordination polymers involving flexible 1,2,4-triazole-based ligands
7 form a promising class of luminescent molecular materials.
8
9
10

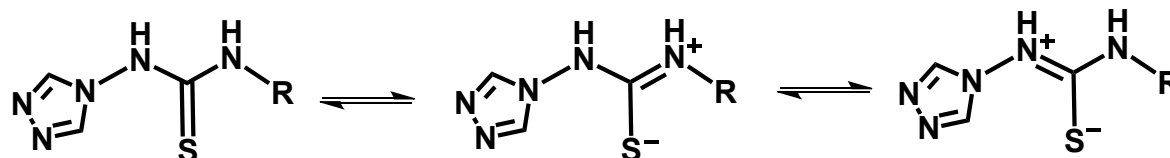
11
12 **KEYWORDS:** Hg(II) coordination compounds, Coordination polymers, 1,2,4-triazole,
13 Thiourea, Hydrogen bonding, DFT, luminescence.
14
15
16
17
18
19
20
21
22
23
24
25
26
27
28
29
30
31
32
33
34
35
36
37
38
39
40
41
42
43
44
45
46
47
48
49
50
51
52
53
54
55
56
57
58
59
60

INTRODUCTION

The journey of 1,2,4-triazole chemistry started with the seminal work by Bladin in 1885.¹ Despite the synthesis of 1,2,4-triazole was established over a century ago, researchers are still working on the design and synthesis of new 1,2,4-triazole compounds,² due for instance to their anti-viral, anti-inflammatory, anti-microbial, and anti-cancer properties.³ The 1,2,4-triazole moieties present in these biologically active compounds justify the criteria's for a potential active drug; for example ribavirin, fluconazole, rizatriptan are the drugs containing 1,2,4-triazole units for treating antiviral, antifungal, and antimigraine infections, respectively.⁴ Inspired by the coordination ability of 1,2,4-triazole ligands to form various coordination network structures, many coordination and material chemists including us⁵⁻¹⁰ developed interesting one (1D), two (2D) and three (3D) dimensional coordination polymer (CP) architectures.¹¹⁻¹³ CPs have been recognized as intriguing porous materials^{14,15} due to their fascinating structures and potential applications were revealed in gas storage,^{16,17} separation,¹⁸ heterogeneous catalysis,^{19,20} spin crossover,^{21,22} drug delivery,²³ theranostics,²⁴ sensors,^{25,26} opto-electronics,²⁷ etc.

Incorporation of hydrogen bonding functionalities (urea, amine, amide, thiourea etc.) within the matrix of a CP is an excellent strategy to create a functional material which can be useful for various applications. In order to synthesize such CPs, two methodologies were used: 1) coordination driven self-assembly of a metal ion with a ligand having programmed hydrogen bonding functionality;²⁸ 2) post-synthetic modification of the CP.²⁹ The resulting functional CP exhibited unprecedented applications in sensor,³⁰ gas storage,³¹ selective CO₂ capture,³² catalysis,³³ selective anion separation,³⁴ etc., and intriguing supramolecular assembled structures by non-covalent hydrogen bonding interactions.²⁸ Moreover, such functionalized CPs showed more competence in their structure dependent applications (for example size-selective hydrogen-bond catalyst³⁵ compared to the non-functionalized CPs).^{28,36-38} Among various organic building blocks, thiourea functionalized ligands attracted many attention, due to their versatile coordination ability towards metal ions through the sulfur or the nitrogen atoms or even through both of them.³⁹ The thiourea moiety exists in two mesomeric forms namely thione and thiolate, and in most of the reported compounds it showed the thiolate form (e.g. on Scheme 1) due to its significant donor strength to the metal ion *via* a coordination bond.^{40,41} Moreover, the

Cambridge structure database (CSD)⁴² search on compounds of thiourea based ligands,^{43,44} showed the presence of characteristic intermolecular N–H...S hydrogen bonding, with dominant N–H...O=C and N–H...S=C hydrogen bond interactions.^{45,46}



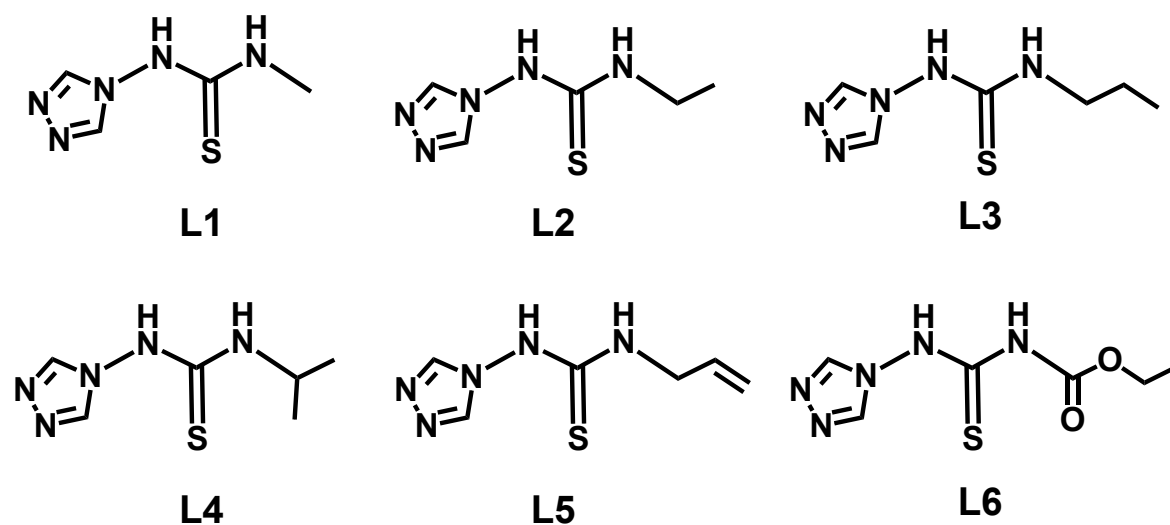
Scheme 1. Mesomeric forms (thione and thiolate) of the ligands L1 – L6 (wherein R = Me, Et, prop, iso-prop, allyl, and COOCH₂CH₃ for L1, L2, L3, L4, L5, and L6 respectively).

Our research in the crystal engineering and functional properties of 1,2,4-triazole ligands,⁴⁷ and their CPs,⁵ led us recently to investigate the structural diversities of two 1,2,4-triazole ligands namely 4H-1,2,4-triazol-4-yl-acetate and 4-(4H-1,2,4-triazol-4-yl)L-propionic acid as a function of the hydrogen bonding functionality attached to the 1,2,4-triazole ligand such as ester and carboxylic acid, respectively.⁴⁷ In these studies, the ester and carboxylic acid moiety functionalized with 1,2,4-triazole, played a significant role for the self-assembly process, which lead to the formation of homochiral helical chains and 2D hydrogen bonded networks, respectively. We have also recently studied the effects of conformational flexibility and hydrogen bonding of the 1,2,4-triazole ligands, on the final outcome of CPs.⁶⁻⁹ In such studies, the 1,2,4-triazole ligand backbone contains hydrogen-bonding carboxylic acid and ester functionalities, which help to interact with solvent molecules and counter anions, and lead to hydrogen bonding assisted self-assembled supramolecular structures. Such compounds showed unusual robustness and thermal stability, and allowed for gas adsorption⁷⁻⁹ and storage of metallic mercury.⁶

Inspired by these functional CPs and their intriguing properties, we decided to functionalize the 1,2,4-triazole with a thiourea moiety (Scheme 1), and study their self-assembly properties as well as their coordination abilities towards the mercury ion due to its enormous negative impact on our environment. This study was also motivated by the following reasons: i) thiourea molecules having nitrogen and sulfur donors atoms have shown their ability to provide variable bonding modes and structural diversity in coordination chemistry.^{48,49} ii) thiourea is expected to participate

1
2
3 to hydrogen bonding interactions with multiple partners (i.e. counter anions, 1,2,4-
4 triazole groups, lattice included or metal bound solvent molecules and even other
5 thiourea functions). iii) nitrogen heteroatoms from the 1,2,4-triazole building block is
6 suitable for coordination with metal ions, and can leads to CP formation. iv) CPs
7 involving triazole-thiourea based ligands have not been reported, and there is no
8 Hg(II) complexes with such ligands reported so far, thus increasing interest of the
9 present report. v) metal-triazole complexes with Hg(II) ions have also been rarely
10 reported.^{50,51} vi) Recently, we have found that for a given complex, the substituents
11 on the ligand and complex counter anions, are important components for modulating
12 luminescent properties of 1,2,4-triazole complexes.⁵¹ We therefore anticipate that the
13 current triazole-thiourea ligands are potential candidates for the detection of Hg by
14 the formation of luminescent complexes, which is environmentally relevant as
15 mercury and its derivatives are known to be highly toxic pollutants.⁵²⁻⁵⁴

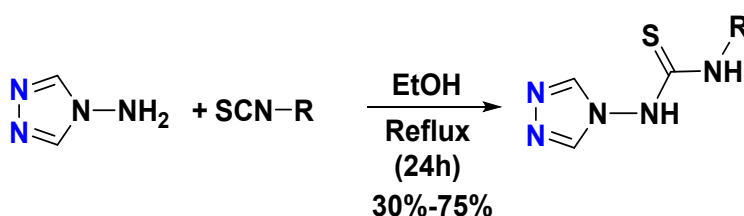
16 In the present account, we introduce the crystal structures of a series of new 1,2,4-
17 triazole ligands functionalized with thiourea **L1** to **L6** (Scheme 2), and their
18 corresponding Hg(II) coordination compounds. We shall explore the effect of
19 hydrogen bonding and metal coordination capability of thiourea functionality of the
20 ligands on the supramolecular structures of the new coordination compounds. We
21 also aim to correlate the luminescent properties of our compounds to their crystal
22 structures. For this purpose, DFT calculations have been performed to assess the
23 nature of the observed emission.



Scheme 2. Chemical structures of the triazole-thiourea based ligands L1 – L6.

RESULTS

Synthesis and General Characterization. The ligands were prepared according to the procedure described by Bielenica *et al.*,⁵⁵ involving reaction of 4-amino-1,2,4-triazole and SCN-R, R being methyl (**L1**), ethyl (**L2**), propyl (**L3**), isopropyl (**L4**), allyl (**L5**), and ethyl formate (**L6**) (Scheme 3). The resulting asymmetric molecules contain a thiourea backbone with 1,2,4-triazole on the other side. This asymmetric nature allows to yield to energetically favorable conformations in their free ligand form and in their coordinated form in Hg coordination compounds.



Scheme 3. Schematic representation of the synthesis of the ligands.

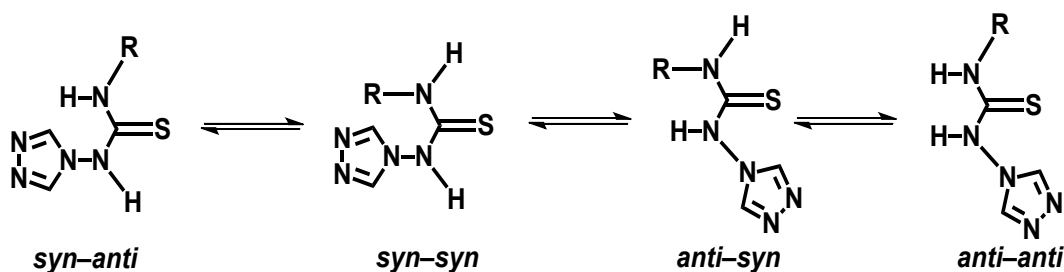
Reaction of such ligands with mercury salts provided ten coordination compounds which were all crystallized, using either slow evaporation or slow diffusion methods (using a branched Γ tube). The compounds were characterized by FT-IR, UV-visible, elemental analysis, and powder X-ray diffraction (PXRD). The compounds were found to be air and light sensitive over time, as well as hygroscopic. The crystal structures of all compounds was determined by single crystal X-ray diffraction (SXRD) providing the following formulae: $\{[\text{Hg}(\mathbf{L1})_2(\mathbf{L1}^-)_2]\}$ (**1**), $\{[(\text{Hg})_2(\mathbf{L1})_2(\mu_2\text{-I})_2(\text{I})_2]\cdot\text{DMSO}\}$ (**2**), $\{[\text{Hg}(\mathbf{L2})(\mu_2\text{-I})\text{I}]\cdot\text{MeOH}\}_\infty$ (**3**), $\{[\text{Hg}_2(\mu\text{-L3})_4]\}_\infty$ (**4**), $\{[\text{HgCl}(\mathbf{L4})\cdot\text{MeOH}]\}$ (**5**), $\{[\text{Hg}_2(\mathbf{L4})_2(\mu_2\text{-I})_2(\text{I})_2]\cdot 2\text{MeOH}\}$ (**6**), $\{[\text{Hg}_2(\mu_2\text{-L5}^-)_4]\}_\infty$ (**7**), $[\text{Hg}_2(\mu_2\text{-Cl})_2(\mathbf{L6}^-)_2(\mathbf{L6}^-)_2]$ (**8**), $\{[\text{Hg}_2(\mu_2\text{-Br})_2(\mathbf{L6}^-)_2(\mathbf{L6}^-)_2]\}$ (**9**), $\{[\text{Hg}_2(\mu_2\text{-I})_2(\mathbf{L6}^-)_2(\mathbf{L6}^-)_2]\}$ (**10**) and $\{[\text{Hg}_2\text{I}_3(\mu_3\text{-L5}')]\}_\infty$ (**11**).

FT-IR spectroscopy. The ligands and coordination compounds were investigated by solid state Fourier Transform infrared spectroscopy (FT-IR) over the range 4000 to 400 cm^{-1} by using KBr pellets. The comparison plots are provided in the Supporting Information (SI). The FT-IR stretching and bending frequencies of ligands and the corresponding coordination compounds showed similarity in the corresponding characteristic peaks. In the FT-IR spectra of **1** and **2**, the band at 3170 and 3134 cm^{-1} , respectively, was found to shift (3109 cm^{-1}) from the corresponding ligand **L1**. This band is attributed to the characteristic thiourea N–H stretching.⁵⁶ The characteristic IR absorption peaks belonging to 1,2,4-triazole ring such as C–H aromatic vibrations (3088 and 2936 cm^{-1} for **L1**, 3089 and 2970 cm^{-1} for **1**, 3109 and 2938 cm^{-1} for **2**), C=C stretching (1520 and 1440 cm^{-1} for **L1**, 1512 and 1498 cm^{-1} for **1**, 1520 & 1444 cm^{-1} for **2**) and –N=N stretching (1572, 1576, and 1572 cm^{-1} for **L1**, **1** and **2**, respectively) were also observed in the FT-IR spectrum of the free ligand **L1** and corresponding complexes **1** and **2**. In addition, the band appearing at 1237 cm^{-1} due to thiourea C=S stretching in the free ligand **L1** was downward shifted to 1210 and 1183 cm^{-1} in the IR spectra of the complexes **1** and **2**, respectively, indicating the coordination through thiourea sulfur atom.⁵⁷ The coordination of Hg(II) with S atom of the thiourea moiety of the ligand was confirmed by the IR band at 571 and 567 cm^{-1} for **1** and **2**, respectively, attributed to the Hg–S stretching frequency. Similarly, the FT-IR spectrum of compounds **3**, **4**, **5**, **6**, **7**, **8**, **9**, **10** and **11**, and their corresponding ligands showed N–H stretching of thiourea, C–H, C=C, and –N=N aromatic stretching vibrations (all the three belong to 1,2,4-thiourea functionality), thiourea C=S, and metal-ligand Hg–S stretching vibrations (Table S5).⁵⁸⁻⁶¹

UV-visible spectroscopy. UV-visible absorption spectra of the molecules **L1-L6** and coordination compounds were recorded in the solid state over the range $\lambda = 200\text{--}800$ nm (Spectra are shown in supporting information). The electronic spectra of ligands showed absorption bands exclusively in the UV region, corresponding to intra-ligand transitions such as $\pi\text{--}\pi^*$ and $n\text{--}\pi^*$. Similar bands were also observed in the spectra of the corresponding coordination compounds, although they were red-shifted.

Single Crystals X-ray Diffraction. Details of the data collection and refinement are given in Table S1. Topological analysis of the nets was performed using the TOPOS program package.^{62,63}

Crystal Structures of Triazole-thiourea Molecules. The ligands **L1** to **L6** are expected to show four possible conformations “*syn-syn*”, “*anti-anti*”, “*syn-anti*”, and “*anti-syn*”, in which the hydrogen atoms of thiourea function near the 1,2,4-triazole ring and alkyl / allyl / ethyl formate are on the same side (or face), opposite side, same and opposite side, opposite and same side, of thiourea, respectively (Scheme 4).



Scheme 4. Plausible conformations of the ligands **L1** to **L6**.

1-methyl-3-(4H-1,2,4-triazol-4-yl)thiourea (L1). The triazole-thiourea molecule **L1** crystallizes in the centrosymmetric monoclinic $P2_1/n$ space group (Table S1). The asymmetric unit contains one molecule of **L1** and one molecule of lattice included water. From the crystal structure, it is found that the ligand is non-planar, in which the triazole ring and the thiourea-methyl functionalities are almost perpendicular to each other [the torsion angle between the triazole and thiourea is $83.35(13)^\circ$], and shows *anti-syn* conformation (Scheme 4). The lattice water molecule stabilizes the structure by hydrogen bond interactions with three neighbouring molecules of **L1**, acting as acceptor for the N-H group of thiourea adjacent to 1,2,4-triazole ring, while hydrogen bonding to both nitrogens of the N-N bond of **L1**, one on each side. A macrocyclic ring structure with graph set notation $R_4^4(14)$ can be constructed involving an N atom the triazole, the N-H of thiourea, and the water molecule [$O\cdots H = 2.926(12)$ Å, $\angle O-H-N = 148.06^\circ$; $N-H\cdots O = 2.741(14)$ Å, $\angle N-H-O =$

153.75°]. Such 0D hydrogen bonded macrocycles interact with each other through hydrogen bonding, resulting in the formation of a 2D hydrogen bonded supramolecular network structure. TOPOS analysis^{62,63} suggests that it is a 2D hydrogen bonded network with Point symbol $\{4.8^2.10^3\}\{4.8^2\}$. The 2D hydrogen bonded network was further packed on top of each other, with the support of N–H···S hydrogen bonding involving thiourea functionalities; N–H···S is dominated by a homosynthon formation between two adjacent thiourea across an inversion centre, forming a $R_2^2(8)$ ring [N–H···S = 3.3752(19) Å, $\angle\text{N–H–S} = 164.46^\circ$] (Figure 1).

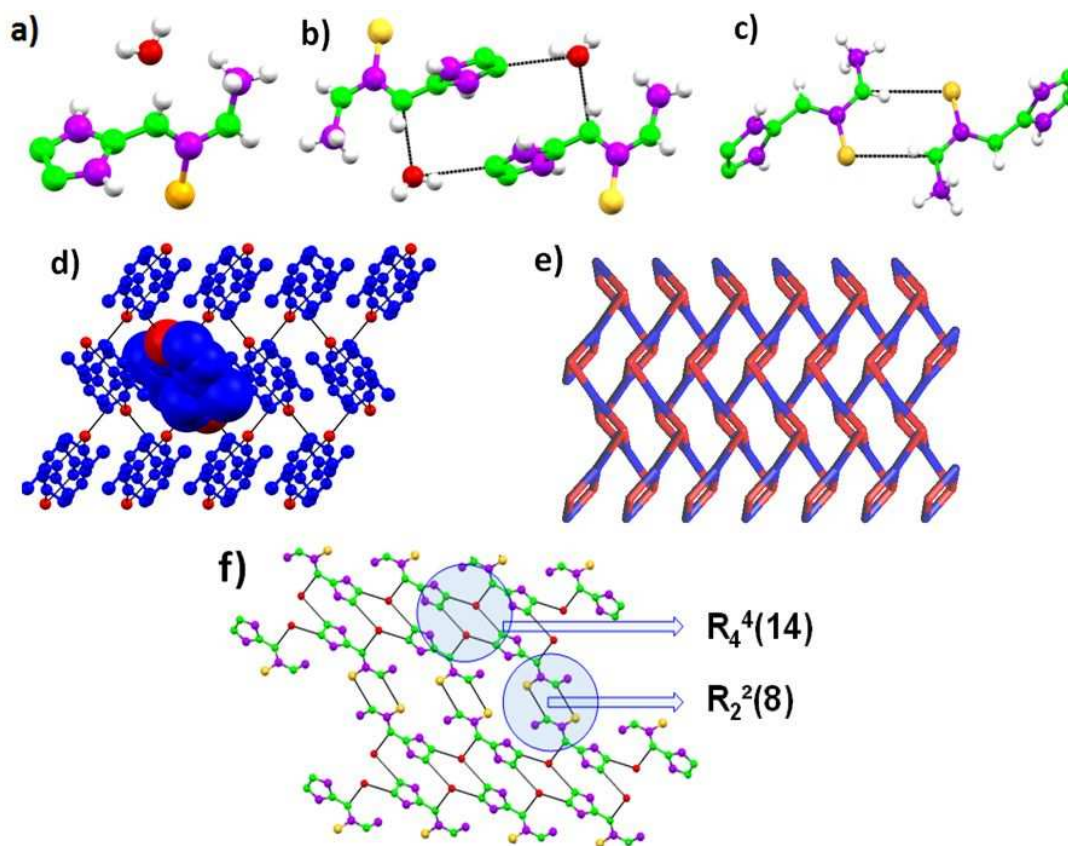


Figure 1. Crystal structure illustration of **L1** – a) asymmetric unit of **L1**; b) 14-membered hydrogen bonded macrocycle with graph set $R_4^4(14)$; c) $R_2^2(8)$ ring formed by the self-complementary thiourea hydrogen bonding; d) 2D hydrogen bonded sheet formed from the self-assembly of hydrogen bonded macrocycles (one of such macrocycles is shown in space fill model); e) TOPOS view of 2D hydrogen bonded sheet; f) parallel packing of 2D hydrogen bonded sheets through thiourea hydrogen bonding, displaying two distinct synthons.

1
2
3
4
5 *1-ethyl-3-(4H-1,2,4-triazol-4-yl)thiourea (L2)*. The ethyl-thiourea derivative of 1,2,4-
6 triazole **L2** also crystallizes in the centrosymmetric monoclinic space group $P2_1/n$
7 (Table S1), with a single molecule in the asymmetric unit. The ligand exhibits a non-
8 planar conformation in which the 1,2,4-triazole ring and the thiourea-ethyl functional
9 groups were found almost orthogonal to each other (torsion angle of 84.29°). Ligand
10 **L2**, showed *syn-anti* conformation (Scheme 4), as opposed to **L1**. As a result the
11 observed homosynthon is formed with the NH adjacent to the triazole moiety ($R_2^2(8)$
12 ring), contrary to **L1** where the other NH group was acting as a donor [$N-H\cdots S =$
13 $3.248(8) \text{ \AA}$, $\angle N-H-S = 165.87^\circ$]. The other NH moiety is equally involved in a ring
14 structure $R_2^2(14)$, linking two molecules through an interaction with a triazole nitrogen
15 [$N-H\cdots N = 2.956(14) \text{ \AA}$, $\angle N-H-N = 152.74^\circ$]. The combination of both interactions
16 leads to the formation of 1D *zig zag* hydrogen bonded chains (Figure 2). Interestingly
17 the adjacent hydrogen bonded chains are packed in parallel fashion sustained by
18 interactions of both triazole C-H hydrogens with a triazole N and the thiourea S atom
19 on either side of the triazole. [$C-H\cdots N = 3.358(6) \text{ \AA}$, $\angle C-H-N = 148^\circ$; $C-H\cdots S =$
20 $3.79(10) \text{ \AA}$, $\angle C-H-S = 153^\circ$], forming a 2D layer expanding in the *ab* plane. In the *c*
21 directions these planes are offset in an almost orthogonal fashion, exposing the
22 hydrophobic ethyl groups to one another.
23
24
25
26
27
28
29
30
31
32
33
34
35
36
37
38
39
40
41
42
43
44
45
46
47
48
49
50
51
52
53
54
55
56
57
58
59
60

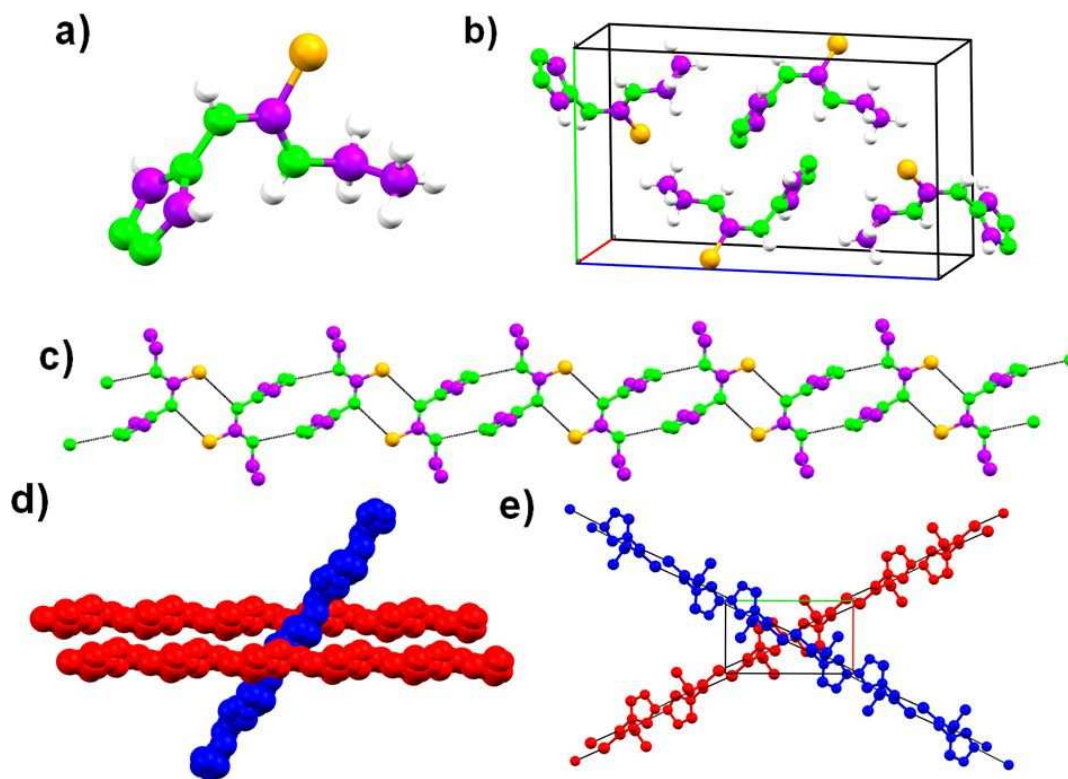


Figure 2. Crystal structure illustration of **L2** – a) asymmetric unit of **L2**; b) crystal packing of **L2** molecules within the unit cell; c) 1D *zigzag* hydrogen bonded chain, around crystallographic axis 'a' (hydrogen atoms were omitted for clarity); d) and e) orthogonal packing of 1D *zigzag* chains (parallel packed 1D chains are shown in red color).

1-propyl-3-(4H-1,2,4-triazol-4-yl)thiourea (**L3**). **L3** equally crystallizes in the centrosymmetric monoclinic space group $P2_1/n$ (Table S1). The asymmetric unit comprises of one molecule of **L3**. The thiourea derivative ligand **L3**, adopts a non-planar geometry with *syn-anti* conformation (Scheme 4) as in **L2**; the triazole ring and thiourea moiety are almost orthogonal to each other with a torsion angle of 84.75° . The *syn-anti* conformation allows an identical $R_2^2(8)$ ring homosynthon as in **L2**, [N–H \cdots S = 3.256(2) Å, \angle N–H–S = 164°]. The $R_2^2(14)$ ring is also observed, similar to **L2** [N–H \cdots N = 2.939(3) Å, \angle N–H–N = 152°]. Such hydrogen bonding leads to the formation of 1D *zigzag* hydrogen bonded chains. While **L3** exhibits similar hydrogen bonding patterns as **L2**, also forming 2D layers, consecutive 2D layers do not show

1
2
3 an orthogonal off-set but rather a parallel displacement between stacked layers in the
4 c direction.
5

6
7 *1-isopropyl-3-(4H-1,2,4-triazol-4-yl)thiourea (L4)*. **L4**, isopropyl analogue and isomer
8 to **L3**, crystallizes in the centrosymmetric triclinic *P*-1 space group (Table S1), with
9 one molecule in the asymmetric unit. **L4** exhibits a non-planar *syn-anti* conformation
10 (Scheme 4) as **L2** and **L3**, in which the triazole and thiourea moiety are orthogonal to
11 each other having a torsion angle of 86.16°. As observed in the crystal structure of
12 **L2** and **L3**, similar hydrogen bond patterns are present: the $R_2^2(8)$ ring involving N-
13 H...S [N–H...S = 3.225(2) Å, \angle N–H–S = 163°] as well as the $R_2^2(14)$ ring [N–H...N =
14 2.999(13) Å, \angle N–H–N = 155.04°]. These hydrogen bonding leads to the formation of
15 a zigzag chain and expansion of the C-H interactions of the triazole also leads to 2D
16 layers, which as in **L3** show parallel displacement between consecutive layers (See
17 Figure S2). A polymorph of **L4** was also obtained (**L4-poly**), also crystallizing in *P*-1,
18 with a slightly larger unit cell volume. On the molecular level, both structures are quite
19 similar, showing similar $R_2^2(8)$ rings between the thiourea groups. Due to subtle
20 conformational differences the $R_2^2(14)$ ring is however formed with the other triazole
21 nitrogen, thus disrupting the 2D layers formed by interactions with the triazole C-H
22 groups. In **L4-poly**, the isopropyl and the adjacent N-H are found disordered over
23 three sites, which might indicate that the $R_2^2(14)$ ring shows less favourable
24 hydrogen bond interactions (Figure S3).
25
26
27
28
29
30
31
32
33
34
35
36
37
38

39 *1-allyl-3-(4H-1,2,4-triazol-4-yl)thiourea (L5)*. The allyl–thiourea derivative of 1,2,4-
40 triazole molecule **L5** crystallizes in the centrosymmetric monoclinic space group
41 $P2_1/n$, with one molecule of **L5** in a general position. (Table S1). The triazole ring and
42 the thiourea functionalities showed non-planar *anti-syn* (See **L1**) conformation
43 (Scheme 4), having a torsion angle between them of around 83.89°. **L5** shows an
44 identical $R_2^2(8)$ ring homosynthon as **L1** [N–H...S = 2.746(10) Å, \angle N–H–S = 141.73°],
45 the interaction with the water molecule of the NH adjacent to the triazole in **L1** is
46 substituted by a hydrogen bond with a neighbouring triazole. This interaction restricts
47 the propagation of hydrogen bond interactions to a wavy 2D layers having a
48 hexagonal grid topology. The 2D sheets are further packed exactly on top of each
49 other along crystallographic axis 'a', sustained by various supramolecular interactions
50
51
52
53
54
55
56
57
58
59
60

involving the triazole, C–H \cdots S [C–H \cdots S = 3.664(8) Å, \angle C–H–S = 160°] and C–H \cdots N [C–H \cdots N = 3.280(2) Å, \angle C–H–N = 155°] (Figure 3).

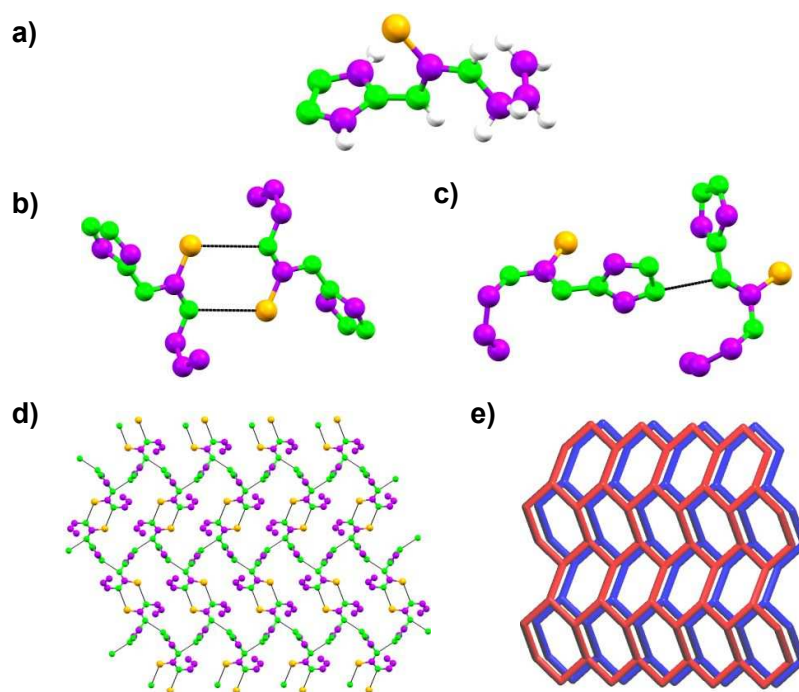


Figure 3. Crystal structure illustration of **L5** – a) asymmetric unit; b) N–H \cdots S with graph set of $R_2^2(8)$; c) N–H \cdots N hydrogen bonding; d) 2D hydrogen bonded sheet formed as a result of N–H \cdots N and N–H \cdots S hydrogen bonding; e) TOPOS view of overall packing of 2D hydrogen bonded networks displaying in various crystallographic axes.

Ethyl 2-(4H-1,2,4-triazol-4-yl)acetate thiourea (L6). **L6** crystalizes in the orthorhombic space group *Pbca* (Table S1), with a single molecule in the asymmetric unit. **L6** exhibits non-planar *anti-syn* conformation (See **L1** and **L5**) (Scheme 4), in which the triazole and thiourea moiety are orthogonal to each other having a torsion angle of 85.68°. In the crystal structure, **L6** molecules lack the $R_2^2(8)$ ring homosynthon involving the S atom, **L6** is rather characterized by a bifurcated hydrogen bond engaged in an intra- and inter-molecular interaction with the carbonyl oxygen of the ester group [N–H \cdots O = 2.642(2) Å, \angle N–H–O = 133° (intra); N–H \cdots O = 3.018(2) Å, \angle N–H–O = 132°]. **L6** undergoes further classical intermolecular hydrogen bonding through thiourea \cdots triazole [N–H \cdots N = 2.854 (2) Å, \angle N–H–N = 165°], and such hydrogen bonding resulted in a hexagonal shaped macrocycle, which is the primary

synthon. Extension of such hydrogen bonding resulted in a 2D hydrogen bonded hexagonal shaped network. The 2D sheets are further packed on top of each other in an offset fashion (along crystallographic axis 'b', sustained by C–H...N [C–H...N = 3.141(4) Å, \angle C–H–N = 121°], involving triazole (C–H)...triazole (N) (Figure 4). A solvate of **L6**, **L6_MeOH** was also found and shows the same bifurcated hydrogen. The MeOH oxygen takes the place of a triazole in the thiourea...triazole hydrogen bond found in **L6**, disrupting the 2D sheets and converting them in a zig-zag layer (Figure S4).

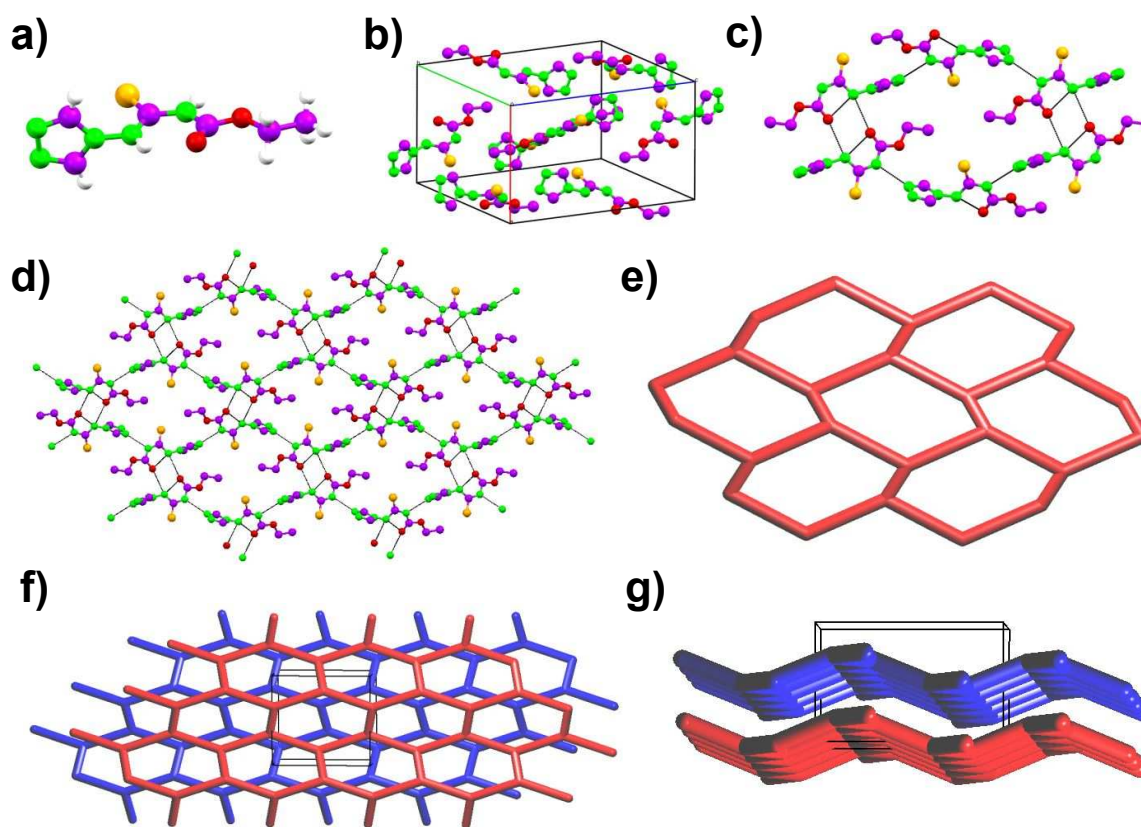


Figure 4. Crystal structure illustration of **L6** – a) asymmetric unit; b) Packing of **L6** molecules in unit cell; c) hexagonal shaped hydrogen bonded macrocycle, sustained by N–H...O and N–H...N hydrogen bonding; d) 2D hydrogen bonded network, formed by the self-assembly of hydrogen bonded macrocycles (along crystallographic axis 'a'); e) TOPOS view of 2D hydrogen bonded network, displaying the hexagon shaped topology; f) and g) Offset packing of 2D sheets along various crystallographic axis.

Table S4 lists the hydrogen bond parameters for the reported ligands and complexes.

Crystal Structures of Coordination Compounds

$\{[Hg(L1)_2(L1^-)_2]\}$ (**1**). Single crystals of complex **1** were grown from MeOH by reacting $Hg(NCS)_2$ and **L1** in 1/3 ratio, and crystallized in the tetragonal space group *I4* (Table S1). The central Hg(II) atom is located on the crystallographic 4-fold axis, with four symmetry equivalent ligands coordinated through the S atoms, without any thiocyanato anions. Thus, the crystal structure of **1**, is described as a mononuclear Hg(II) complex, tetra-coordinated by **L1**, having the formula $\{[Hg(L1)_2(L1^-)_2]\}$. Charge neutrality was indeed achieved by deprotonation of two ligands; as the four ligands are crystallographically identical the charge is spread out over all four ligands and the N-H hydrogen next to the triazole is refined as half occupied. The ligand was found to be disordered over two positions [site occupancy factor = 0.69462 and 0.30538]. The major part shows the “*syn-anti*” conformation as in the free ligand, while the minor part is found in the “*anti-anti*” conformation (Scheme 4). In the crystal structure of **1**, ligand **L1** displays an orthogonal arrangement between triazole–thiourea (dihedral angle of 89.76°) in the major part, the minor part shows a more planar structure with a dihedral angle of 21.02° . The coordination around Hg(II) for the major and minor part is best described as a near perfect square pyramid ($\tau_4 = 0.95$ and 1.08 , respectively). We recall that $\tau = 0$ for square pyramidal and $\tau = 1$ for trigonal-bipyramidal arrangement), with τ is defined by the ratio $(\beta - \alpha)/60^\circ$ where $\beta > \alpha$ are the two greatest angles of the coordination centre.⁶⁴

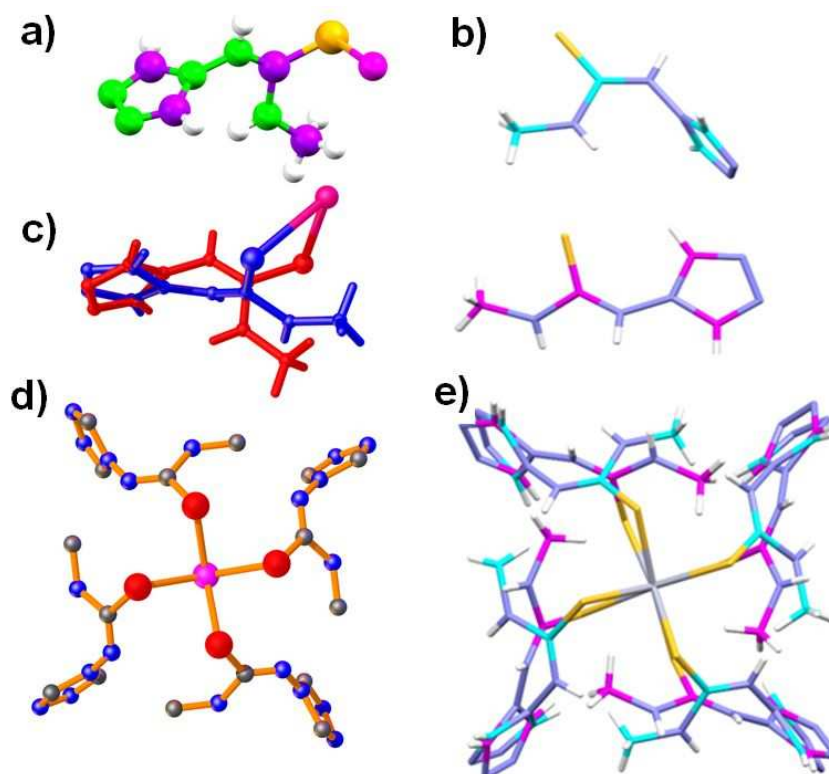
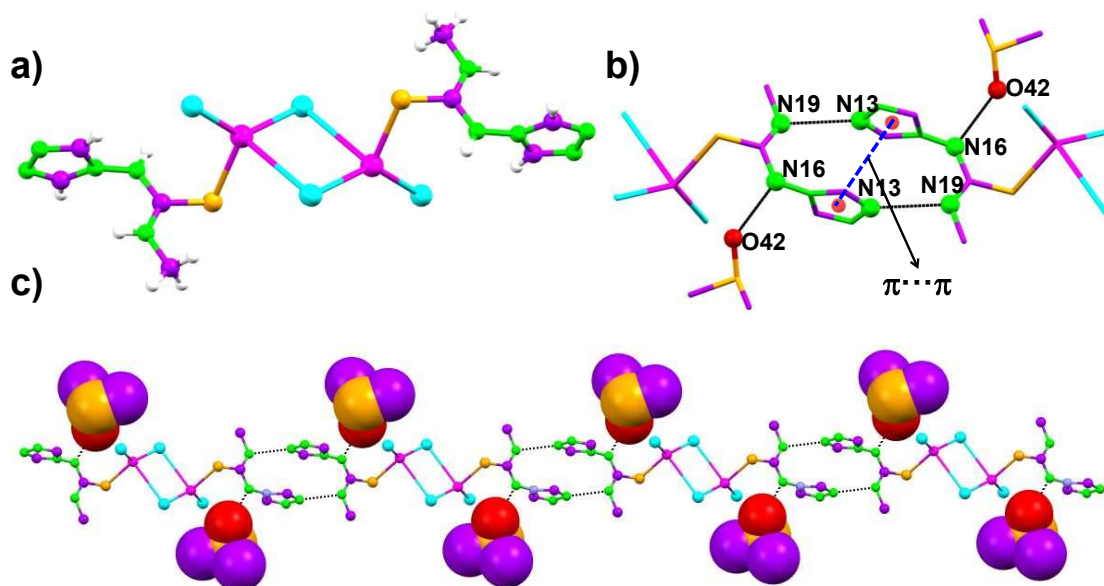


Figure 5. Crystal structure illustration of **1** – a) asymmetric unit; b) Stick representation of the ligand as observed in **1**; major part in cyan, minor part in magenta; c) disorder of the ligand molecule over two positions (shown in red and blue color, Hg(II) is shown in magenta); d) mononuclear Hg(II) complex with 1:4 metal to ligand stoichiometric ratio with coordinated sulfur atoms in red. e) **1** showing the observed disorder.

$\{[Hg_2(L1)_2(\mu_2-I)_2] \cdot DMSO\}$ (**2**). The Hg(II) binuclear complex **2**, which was prepared by reacting HgI_2 and **L1** in MeOH, crystallized in the centrosymmetric triclinic $P\bar{1}$ space group (Table S1). The unit cell contains one binuclear complex, found on an inversion centre and two non-coordinated molecules of dimethyl sulfoxide (DMSO). Two iodine anions are bridging the two Hg(II) centres, and the trigonal pyramidal ($\tau_4 = 0.78$) coordination is further completed by a third iodine anion, and one molecule **L1**, coordinated through the thiourea sulfur atom. Ligand **L1** displays a non-planar geometry with a “*syn-anti*” conformation (Scheme 4), contrary to the *anti-syn* conformation of the free ligand and shows a dihedral angle of 88.19° , between thiourea and triazole ring. The Hg(II) binuclear complex exhibits N–H \cdots N hydrogen bonding [N–H \cdots N = $2.861(2)$ Å, \angle N–H–N = 152.92°] between the thiourea and

1
2
3 triazole, resulting in a 1D hydrogen bonded chain, leading to the formation of a
4 fourteen-membered hydrogen bonded macrocycle of graph set $R_2^2(14)$. Additionally,
5 $\pi \cdots \pi$ stacking interactions are present in this macrocycle between 1,2,4-triazole
6 moieties [distance between the triazole ring centroids = 3.506 Å]. The N-H adjacent
7 to the triazole shows a hydrogen bond to the DMSO oxygen (Figure 6).
8
9



33 **Figure 6.** Crystal structure illustration of **2** – a) binuclear Hg(II) complex displaying
34 the bridging of iodide anions between the Hg(II) ions; b) hydrogen bonding and $\pi \cdots \pi$
35 stacking interactions in **2**; c) 1D hydrogen bonded chain sustained by N-H \cdots N
36 hydrogen bonding, displaying the occlusion of DMSO (space fill model) within the
37 interstitial space.
38
39
40
41
42

43 $\{[Hg(\mathbf{L2})(\mu_2\text{-I})] \cdot \text{MeOH}\}_\infty$ (**3**). The coordination polymer **3**, which was prepared by
44 reacting HgI_2 and **L2** in 1/1 ratio in a MeOH/THF mixture, crystallized in the
45 monoclinic space group $P2_1/c$ (Table S1). The asymmetric unit comprises one Hg(II),
46 one molecule of **L2**, two iodide anions (both **L2** and iodide are coordinated to the
47 metal center), and one molecule of lattice included methanol (MeOH) entrapped in
48 the crystal lattice. The Hg(II) metal center shows a distorted trigonal pyramidal
49 geometry [$\tau_4 = 0.77$] in which three positions are coordinated by iodide anions and
50 the fourth coordination site is occupied by a S atom of the thiourea functionality of
51
52
53
54
55
56
57
58
59
60

ligand **L2**. Two positions of the iodine atoms around every Hg(II) centre are symmetry related, resulting in extended coordination polymerization, which leads to the formation of a 1D coordination polymer. This type of 1D coordination chains of $\{-\text{Hg}-\text{I}-\text{Hg}-\text{I}-\text{Hg}-\}_{\infty}$ is commonly found in Hg(II) CPs.^{65,66} The ligand showed near identical conformation as in the free ligand **L2** (*syn-anti* conformation, RMSD 0.37Å between the free and complexed **L2** ligand) and a similar $R_2^2(8)$ ring homosynthon as in the free **L2** ligand interactions [$\text{N}-\text{H}\cdots\text{N} = 2.977(6)$ Å, $\angle\text{N}-\text{H}-\text{N} = 151.29^\circ$], resulting in the formation of 2D hydrogen bonded corrugated sheet like architecture. The $\pi\cdots\pi$ stacking interactions involving the 1,2,4-triazole rings further strengthen this 2D corrugated sheets [centroid \cdots centroid = 3.448 Å]. In the crystal structure, the lattice included MeOH molecule is found to be hydrogen bonded with thiourea nitrogen atom of the 2D sheet, and 1,2,4-triazole nitrogen atom of adjacent 2D sheet [$\text{N}-\text{H}\cdots\text{O} = 2.729(12)$ Å, $\angle\text{N}-\text{H}-\text{O} = 143.95^\circ$; $\text{O}-\text{H}\cdots\text{N} = 2.823(8)$ Å, $\angle\text{N}-\text{H}-\text{O} = 179.68^\circ$]; this hydrogen bonding leads to the formation of a 3D hydrogen bonded network structure (Figure 7).

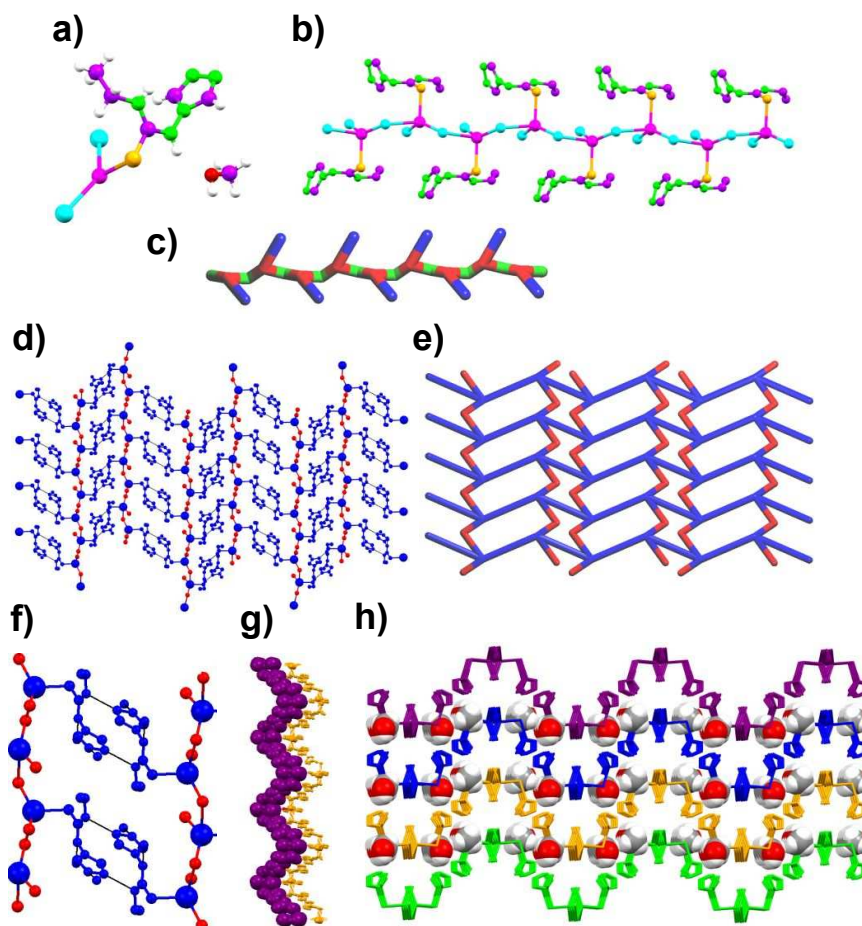
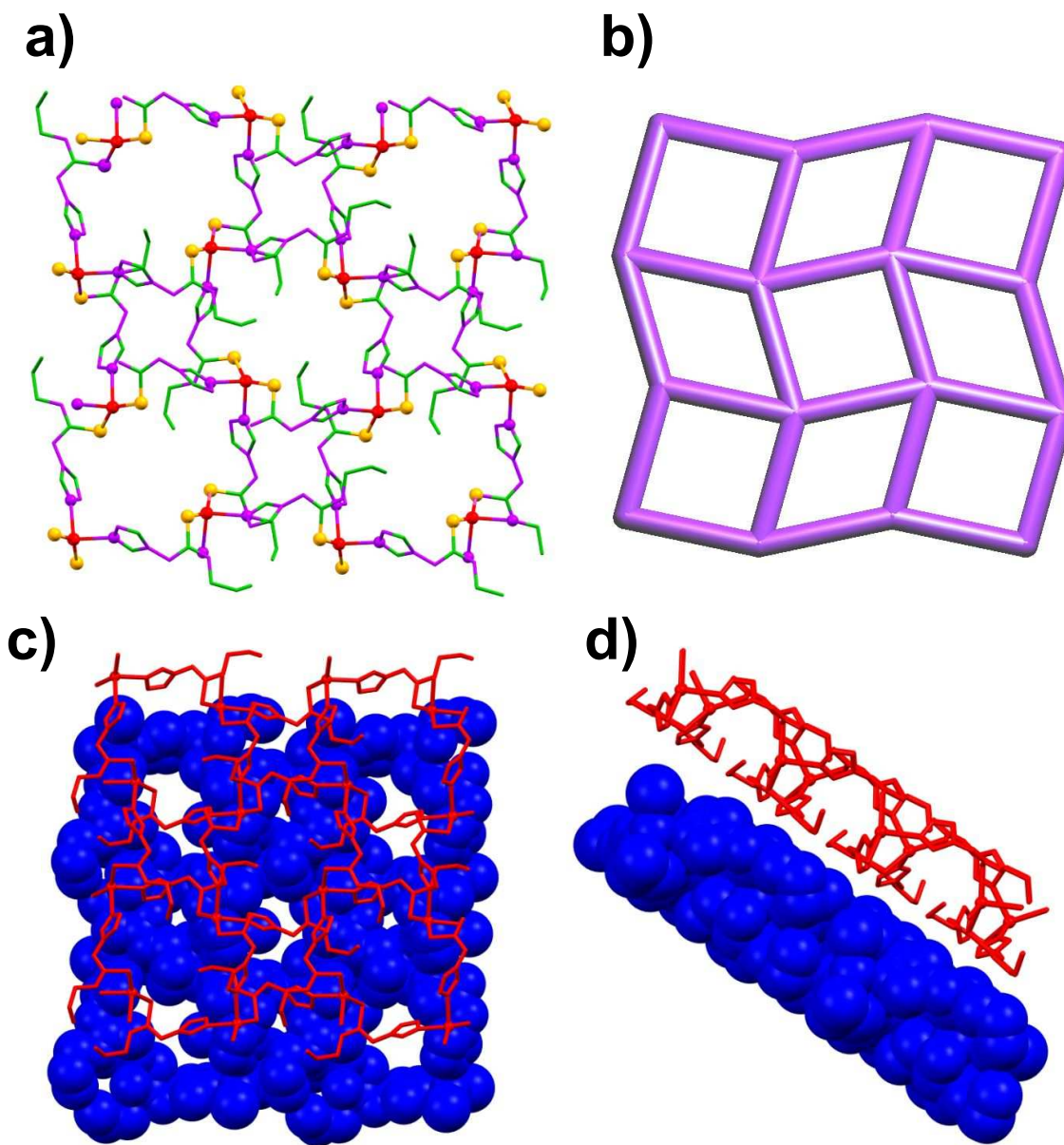


Figure 7. Crystal structure illustration of **3** – a) asymmetric unit containing the monomer unit of CP **3**, and lattice included MeOH; b) 1D CP displaying the $\{-\text{Hg}-\text{I}-\text{Hg}-\text{I}-\text{Hg}-\}$ units (Hg and I atoms are shown in magenta and cyan color, respectively), and apically coordinated ligand **L2**; c) TOPOS view of the backbone of the CP (Hg, I and N atom of triazole are shown in red, green, and blue color); d) Extension of 1D CP to 2D hydrogen bonded corrugated sheet structure sustained by N–H \cdots N and $\pi\cdots\pi$ stacking interactions; e) TOPOS view of 2D sheet; f) a close look of N–H \cdots N hydrogen bonding; g) parallel packing of 2D corrugated sheets (adjacent sheets are shown in purple and orange color); h) overall packing of 2D sheets, displaying the inclusion of MeOH (shown as space fill model) within the interstitial space of the sheets (adjacent sheets are shown in purple, blue, orange and green).

$\{[\text{Hg}_2(\mu\text{-L3})_4]\}_\infty$ (**4**). Single crystals of the coordination polymer **4**, which was prepared by reacting HgCl_2 and **L3** in MeOH in a 1/1 ratio, belong to the monoclinic space group Pn (Table S1). The asymmetric unit contains two crystallographically independent Hg(II) ions and four crystallographically independent ligand molecules. The Hg(II) centers coordinate to four **L3** ligands through N and S atoms of 1,2,4-triazole and thiourea moieties, respectively, bridging the metal centres in all directions. The propyl group of two ligand molecules is disordered over two positions. The metal center displays a slightly distorted trigonal pyramidal geometry [$\tau_4 = 0.77$ and 0.73]. While HgCl_2 was used as starting salt, the crystal structure does not contain any chloride anions. Actually, a closer look on the crystal structure revealed that the positive charges of Hg(II) are balanced by the deprotonated form of ligand **L3** (the deprotonation takes place from the thiourea N–H, adjacent to triazole ring). The N–N bond length involving the triazole N atom and thiourea N atom showed a slight increase from $1.386(2)\text{\AA}$ in the free ligand to a range of $1.394(8)$ – $1.416(11)\text{\AA}$ in the CP, further confirming the deprotonation. The ligand **L3** exhibits *anti-syn* conformation, contrary to the free ligand that showed the *syn-anti* conformation, in which the dihedral angle between thiourea and triazole ring are in the range of 64.03° – 78.41° . The extended coordination of **L3** with Hg(II) resulted in the formation of a 2D square grid coordination polymer with corrugated sheet like architecture. The

1
2
3 thiourea N-H exhibits intra molecular hydrogen bonding with the N atom of 1,2,4-
4 triazole (see supporting information), which further stabilize the 2D corrugated sheet.
5 Such sheets are packed on top of each other along crystallographic axis 'a' in slight
6 offset fashion, supported by various supramolecular interactions (Figure 8).
7
8
9



51
52
53
54
55
56
57
58
59
60

Figure 8. Crystal structure illustration of **4** – a) 2D corrugated square grid CP, displaying the distorted trigonal pyramidal geometry of Hg(II) and the coordination modes of ligand **L3**; b) TOPOS view of 2D corrugated square grid CP; offset packing

of the square grid CPs along crystallographic axis 'a' c) and 'b' d) (adjacent CPs are shown in blue and red color).

$\{[HgCl(L4)L4] \cdot MeOH\}$ (**5**). Single crystals of the complex **5** formed by the reaction of $HgCl_2$ and **L4** in 1/1 ratio in a MeOH/THF mixture, belong to the centrosymmetric triclinic space group *P*-1 (Table S1). The asymmetric unit contains two crystallographically independent Hg atoms, each of which is coordinated to two molecules of **L4** (through the S atom of the thiourea) and to one chloride anion [Hg–Cl = 2.541(11)-2.548(8) Å; Hg–S = 2.395(5)-2.409(5)] in a distorted trigonal planar geometry, forming a mononuclear complex. For one of the discrete complexes **5**, both **L4** isopropyl groups were found disordered over two positions. The four MeOH solvent molecules found in the unit cell are also disordered over two sites. Bond valence analysis indicates that both Hg centres are in the II+ state, for which the charges are counter balanced by one Cl anion and a deprotonated **L4**⁻ ligand. In all **L4** ligands, the N atom adjacent to the triazole is deprotonated and all show the *anti-syn* conformation, contrary to the free ligand that was found in the *syn-anti* conformation, but in one of the two **L4** ligands on every Hg centre the 1,2,4-triazole is protonated, forming a hydrogen bond with the deprotonated triazole of a symmetry related complex, in a $R_2^2(28)$ ring [N–H⋯N = 2.71(3)Å, $\angle N-H-N = 161^\circ$ or N–H⋯N = 2.70(3)Å, $\angle N-H-N = 157^\circ$]. The complexes are further stabilized by intra-molecular hydrogen bonds between the thiourea N-H and the Cl atom. The formation of the hydrogen bonded macrocycles results in two solvent channels running along the *a*-axis. In both channels, disordered MeOH molecules are located. The disordered nature of the MeOH molecules and the absence of any interactions with the complexes suggests that the MeOH molecules might migrate through the channels (Figure 9).

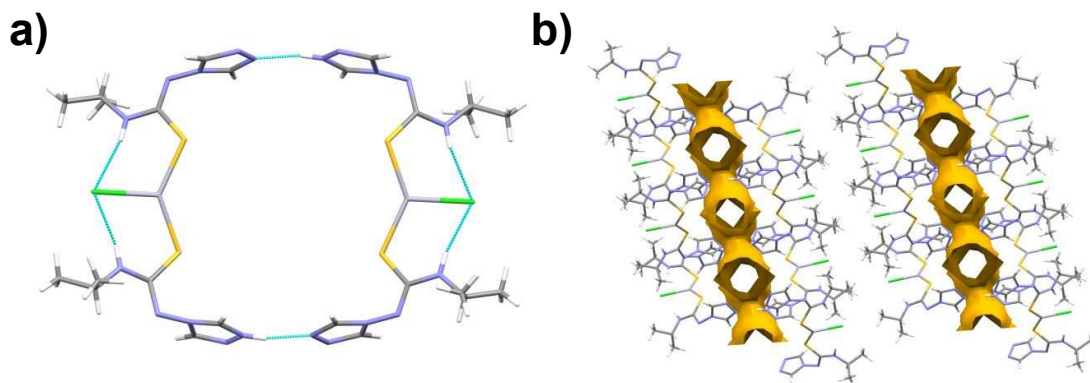


Figure 9. a) $R_2^2(28)$ ring macrocycle formed by hydrogen bond interactions, showing intramolecular hydrogen bonds with the chlorine atom (green) in **5**. b) solvent channels shown where the disordered MeOH molecules are located.

$\{[Hg_2(L4)_2(\mu_2-I)_2] \cdot 2MeOH\}$ (**6**). **6** which was prepared by reacting HgI_2 and **L4** in a 1/1 ratio in a MeOH/THF mixture, crystallizes in a centrosymmetric triclinic space group $P-1$ (Table S1), revealing a binuclear complex formed by the self-assembly of Hg(II) salt of iodide and **L4**. The unit cell comprises a single complex **6**, with two μ_2 bridging iodine atoms and two lattice MeOH molecules. The Hg(II) metal center showed distorted tetrahedral geometry [$\tau_4 = 0.79$], in which three coordination sites are occupied by iodide anions and the remaining fourth was coordinated with S atom of the ligand **L4**. The ligand **L4** showed *syn-anti* conformation as in the free ligand **L4**; the dihedral angles involving the thiourea and triazole ring being 78.73° . As in the free ligand **L4**, the N atoms of the 1,2,4-triazole group of **L4** form a homo dimer synthon ($R_2^2(14)$ ring) (Figure 10) [$N-H \cdots N = 3.057(6)$ Å, $\angle N-H-N = 144.39^\circ$], expanding into a 1D chain, which are held together by the lattice MeOH solvent molecules.

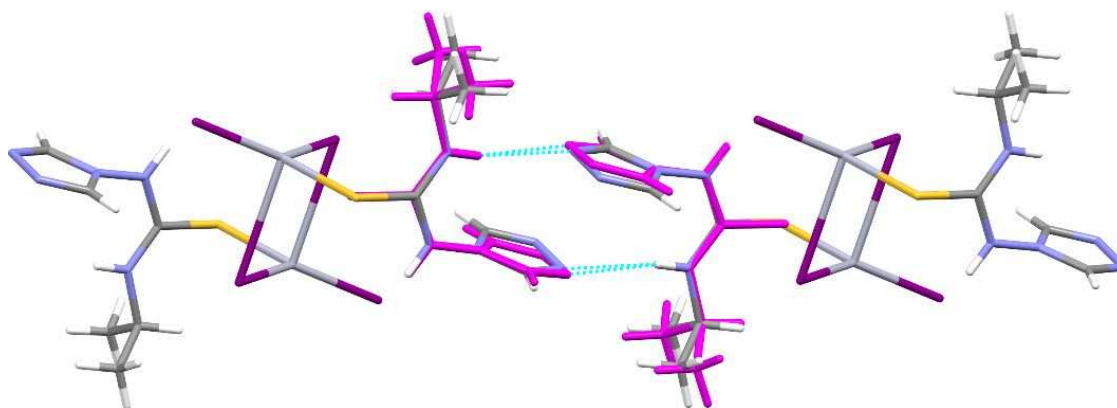


Figure 10 Stick representation of **6** showing identical hydrogen patterns as in the free ligand **L4** (superposed in magenta).

$\{[Hg_2(\mu_2-L5^-)]_4\}_\infty$ (**7**). Single crystals of the coordination polymer **7**, which were prepared by reacting $HgCl_2$ and **L5** in 1/1 ratio in a mixture of MeOH/THF, crystallized in the monoclinic space group Pn and displayed similar cell dimensions and packing as observed in **4** (Table S1). Ligands **L5** and **L3** show the same conformation in **7** and **4**, respectively and the small conformational differences between the isostructural complexes are located between the allyl or propyl moieties. Figure 11 shows the superposition of **7** and **4**, with near perfect overlap.

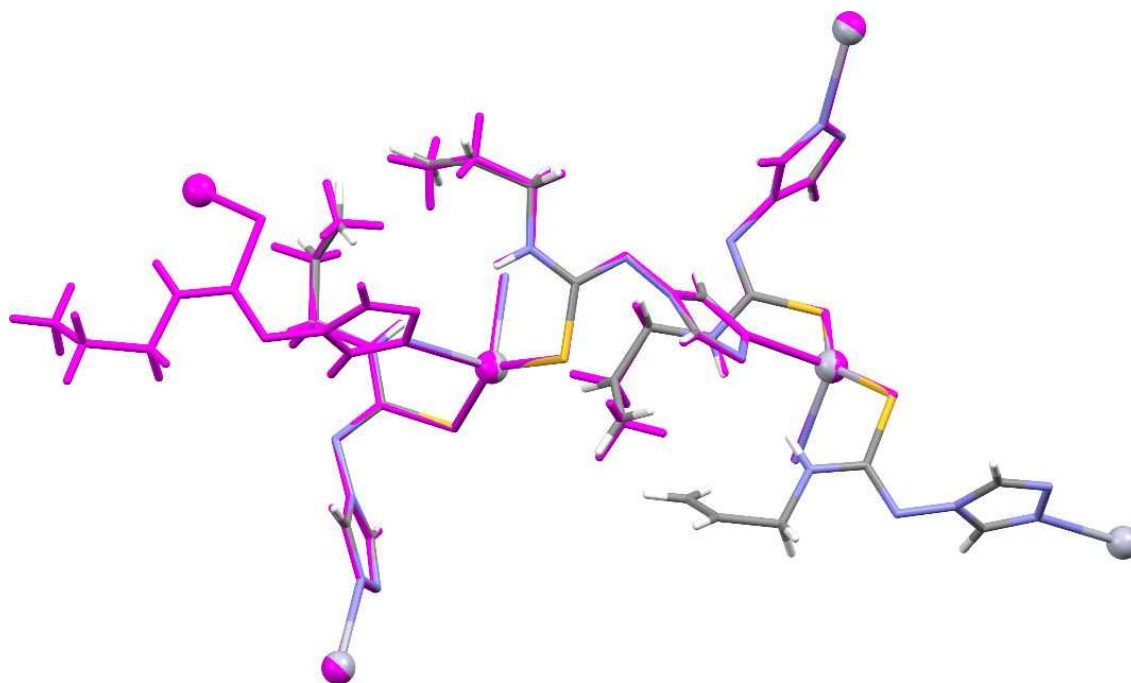


Figure 11 Superposition of **7** onto **4** (magenta), showing near perfect overlap, also between the ligands **L5** (allyl) and **L3** (propyl).

$[Hg_2(\mu_2-Cl)_2(L6^-)_2(L6)_2]$ (**8**), $\{[Hg_2(\mu_2-Br)_2(L6^-)_2(L6)_2]\}$ (**9**) and $\{[Hg_2(\mu_2-I)_2(L6^-)_2(L6)_2]\}$ (**10**). The single crystals of **8**, **9** and **10** were obtained by the reaction of **L6** with $HgCl_2$, $HgBr_2$, and HgI_2 , respectively, in a 1:1 metal–ligand stoichiometric ratio. Structure determination revealed that the structures of **8**, **9** and **10** are isomorphous, and crystallized in centrosymmetric triclinic space group $P-1$ (Table S1). The unit cell contains a single binuclear complex with two (μ_2) bridging halide anions and two S-coordinated **L6** ligands on either Hg atom (Figure 12). One of the **L6** ligands is in the *anti-anti*, the other in the *anti-syn* conformation, in which the triazole ring and thiourea

moieties are almost perpendicular with dihedral angles of 78.57° & 88.20°, 80.63° & 86.21°, and 82.42° & 87.50°, for **8**, **9**, and **10** respectively. The ligand in the *anti-anti* conformation is deprotonated as **L6⁻** to maintain the charge balance of the Hg(II) metal. The Hg coordination is described as a distorted to near perfect trigonal pyramid [$\tau_4 = 0.79$ (**8**), $\tau_4 = 0.82$ (**9**), $\tau_4 = 0.84$ (**10**)]. The binuclear complex self-assembled into a 3D hydrogen bonded network structure, the main hydrogen bonds involve a dimeric $R_2^2(8)$ ring between the thiourea moieties of neighboring deprotonated **L6** ligands [$N-H\cdots N = 2.995(4)\text{\AA}$, $\angle N-H-N = 150.34^\circ$]. The 3D network is further completed by 1D hydrogen bonded chains in the other directions with the support of $N-H\cdots N$ interactions [$N-H\cdots N = 2.669(11)\text{\AA}$, $\angle N-H-N = 171.4^\circ$] between triazole groups and between the thiourea NH of a protonated and a triazole N of a neutral **L6** [$N-H\cdots N = 2.970(7)\text{\AA}$, $\angle N-H-N = 166.84^\circ$]. Hydrogen bonds for **9** and **10** are reported in the supporting information.

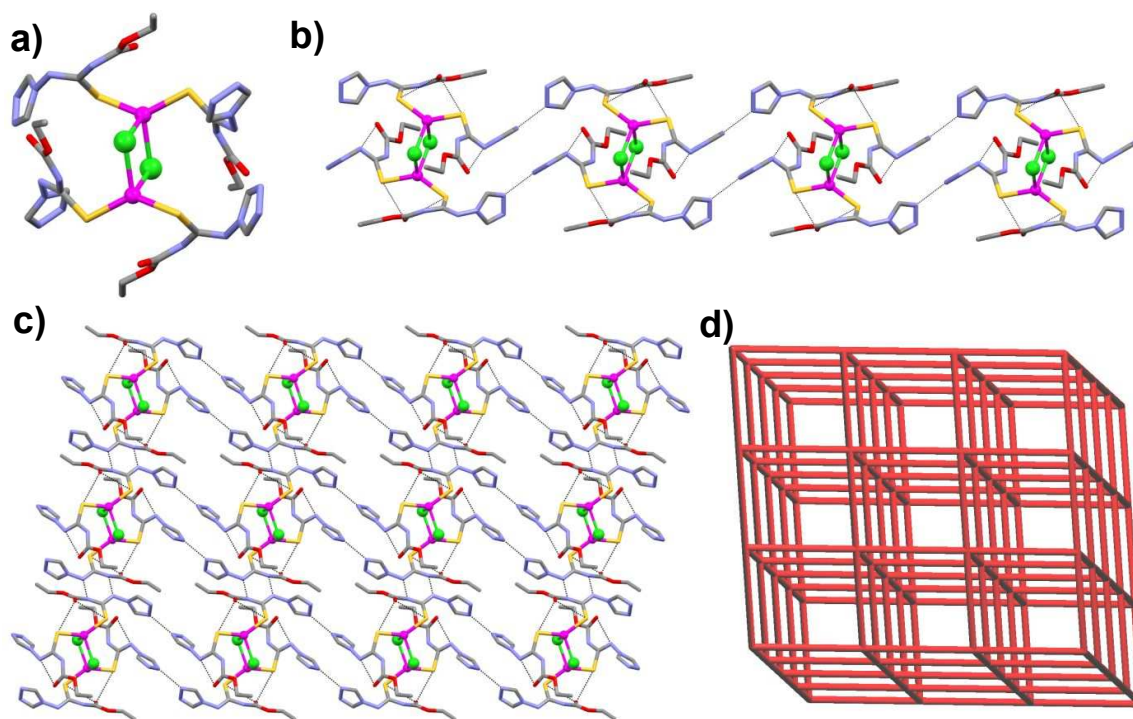


Figure 12. Crystal structure illustration of **8** – a) Hg(II) binuclear complex **8**; b) 1D hydrogen bonded chain; c) 2D hydrogen bonded sheet; d) TOPOS view of 3D hydrogen bonded network structure. Disorder on the alkyl chain was omitted for clarity.

1
2
3 $\{[Hg_2(\mu_3-L5')I_3]\}_\infty$ (**11**). The reaction of allyl substituted thiourea–triazole ligand **L5**
4 with HgI_2 resulted in block shaped colorless single crystals of **11**. SXR D analysis
5 revealed that crystals of **11** belong to the centrosymmetric monoclinic space group
6 $P2_1/c$ (Table S1). Surprisingly, no **L5** was detected in the asymmetric unit. Instead, a
7 five membered cyclic derivative of the 1,2,4–triazole ligand (5-ethyl-1-(4H-1,2,4-
8 triazol-4-yl)imidazolidine-2-thione, **L5'**) coordinated to two Hg metal center, was
9 present, forming a 1D coordination polymer. Three coordinated iodide anions
10 complete the asymmetric unit. The formation of **L5'** is presumably due to a two-step
11 cyclization process in which **L5** reacted with HgI_2 to form a complex in the initial step,
12 and further nucleophilic attack of $[HgI]^+$ on the allylic group (Hg–C bond) resulted in
13 **L5'**. The proposed mechanism of the cyclization process is shown in Scheme S1.
14 The four coordinated Hg(II) metal center shows a distorted trigonal pyramidal
15 geometry ($\tau_4 = 0.78$), with two iodine and a thiourea S atom at the equatorial
16 positions and the triazole N atom in the apical position; the C–Hg–I bond angle is near
17 linear, $177.3(9)^\circ$. The Hg–I distance confirmed the oxidation states of Hg with 2.606–
18 2.657 Å. The positive charges of the Hg are balanced by the coordinated iodide as
19 well as the δ^+ charge on the allylic carbon atoms coordinated to Hg(II) ions. While
20 one Hg(II) metal center shows distorted trigonal pyramidal geometry [$\angle N-Hg-I =$
21 $97.2(3)–101.5(3)^\circ$; $\angle I-Hg-I = 143.45(6)^\circ$; $\angle N-Hg-S = 89.0(3)^\circ$; $\angle I-Hg-S =$
22 $105.55(10)–105.93(10)^\circ$], the Hg(II) ion coordinated to an allylic carbon atom displays
23 a distorted linear geometry [$\angle C-Hg-I = 177.3(9)–177.3(9)^\circ$]. On the other hand, the
24 trigonal pyramidal coordination geometry of Hg(II) is surrounded by N atom of the
25 triazole (apical position) of **L5'**, two iodide and S atom thiourea of ligand **L5'**
26 (equatorial positions). The iodide anions do not participate in any bridging
27 coordination. The extended coordination of N and S atoms of the triazole and
28 thiourea functionalities of **L5'** with both Hg atoms leads to the formation of a 1D CP.
29 In **L5'** the twist angle between the 5-membered rings is about 73° and the bend
30 character leads to the formation of a 1D zigzag CP along the two–fold screw axis
31 (Figure 13).
32
33
34
35
36
37
38
39
40
41
42
43
44
45
46
47
48
49
50
51
52
53
54
55
56
57
58
59
60

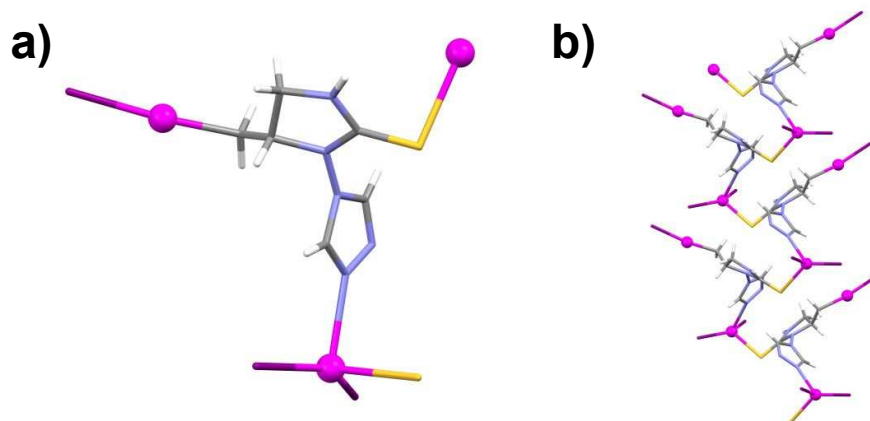


Figure 13. Crystal structure illustration of **11** – a) extended asymmetric unit showing the trigonal pyramidal and linear geometry around the Hg atoms, as well as coordination of **L5'**; b) 1D zigzag CP along the 2₁-axis.

Photoluminescent properties

Emission and excitation spectra of compounds **1–11**, as well as those of corresponding organic ligands, **L1–L6** were investigated in the solid-state. Under UV-vis light excitation at room temperature, none of these samples exhibit distinct photoluminescent signal. This is in contrast to the previously reported series of d¹⁰-metal (Zn(II), Cd(II), Hg(II)) complexes and the related coordination polymers bearing 1,2,4-triazole-based ligands substituted at the 4-position with phenyl-containing groups⁵¹. In the reported case, both free organic ligands as well as the subsequent coordination compounds showed room-temperature blue to blue-green photoluminescence originating from diverse emissive states, mainly related to ligand-centered electronic transitions. This can be correlated herein with the structure of **L1–L6** ligands which also contain the 1,2,4-triazole groups but the remaining organic parts do not contain the aromatic rings which could result either in the larger π -conjugated moieties leading to strongly emissive intra-ligand charge transfer (ILCT) states or in the appearance of emissive ligand-to-ligand charge transfer (LLCT) states occurring thanks to the favorable supramolecular arrangement of ligands neighboring in the crystal lattice. Despite these limitations, a distinct photoluminescence was however detected for compounds **7**, **10** and **11** which all contain binuclear units, as well as in the corresponding free organic ligands, **L5** and **L6**, after cooling the samples to 77 K (Figures 14–16).

1
2
3 Under UV light excitation, compound **7** exhibits broad emission centered at $\lambda = 420$
4 nm with a shoulder around $\lambda = 520$ nm (Figure 14, Table S6). This luminescence is
5 hypsochromically shifted when compared with the free ligand, **L5** showing the broad
6 emission bands at $\lambda = 450$ nm or $\lambda = 518$ nm, depending on the excitation
7 wavelength (Figure 14, Table S6). The ligand **L5** is built of the 1,2,4-triazole group
8 substituted at the 4-position with the thiourea moiety finishing with the well-separated
9 terminal allyl group (Scheme 2). Thus, the occurrence of the ILCT states can be
10 rather excluded. Moreover, the crystal structure of **L5** (Figure 3) does not suggest the
11 formation of supramolecular aggregates involving aromatic 1,2,4-triazole groups
12 which could lead to the LLCT emission. Therefore, the observed photoluminescence
13 of **L5** can be attributed to the classical ligand-centered (LC) fluorescence involving
14 mainly the triazole π -electron system only modulated by the complex substituent.
15 The typical UV excitation of **L5** at $\lambda = 370$ nm produces green emission related to the
16 broadband centered at $\lambda = 520$ nm while the deeper UV light of $\lambda = 270$ nm results in
17 another emission band with the maximum at ca. $\lambda = 450$ nm. These emission signals
18 can be ascribed to two different isolated LC states as clearly visible in two
19 distinguishable bands in the excitation spectrum. A similar excitation pattern was
20 observed for the analogous ligand of *N*-(1,2,4-triazol-4-yl)pyridine-3-carboxamide
21 bearing aromatic triazole and pyridine moieties well separated by the carboxamide
22 group.⁵¹ Such a two-maxima character of the excitation spectrum remains after the
23 coordination of **L5** by Hg(II) metal centers within the 2-D coordination polymer of **7**.
24 Therefore, the resulting emission of **7** can be assigned to the LC transitions as the
25 formation of supramolecular aggregates of **L5** ligands, which could lead to the
26 emissive LLCT states, is not observed in the crystal structure of this coordination
27 network (Figure 11). Both the excitation bands as well as the resulting emission
28 signals of **7** are significantly blue-shifted when compared with free ligand **L5** (Figure
29 14). It can be explained by the strong conformational modification of the ligand upon
30 metal coordination as well as the generation of the deprotonated form of **L5**⁻ which
31 balances the positive charge of Hg(II) metal centers.⁶⁷ As a result, the CIE 1931
32 chromaticity parameters of the ligand **L5** emission of (0.228, 0.494) dramatically
33 changes to (0.215, 0.216) for the luminescent signal of **7** which gives the emission
34 color shift from green to blue (Figure S1 and Table S6). Despite the strong
35 suggestions on the LC origin of the emission in **7**, one cannot exclude the
36
37
38
39
40
41
42
43
44
45
46
47
48
49
50
51
52
53
54
55
56
57
58
59
60

1
2
3 contribution of the ligand-to-metal charge transfer (LMCT) states which are
4 accessible for Hg(II) complexes.^{68,69}
5

6
7 The clarification of the emission mechanism in **7** is enabled by the theoretical
8 calculations of the electronic densities of states (Figure 19b, see next section). The
9 highest occupied states are mainly assignable to the LC electronic states. On the
10 contrary, the lowest unoccupied states contain the main contribution from the ligand
11 states, however, there is a non-negligible contribution from the Hg(II) electronic
12 states. Therefore, the lowest energy optical transition, which is responsible for the
13 observed emission pattern, can be described as the mixture of LC and LMCT (**L5** to
14 Hg(II)) transitions. This assignment explains also the observation of a few
15 overlapping emission components at ca. $\lambda = 400, 450$ and 540 nm, accompanied
16 with the tail towards higher wavelengths (Figure 14).
17
18
19
20
21
22
23
24
25
26
27
28
29
30
31
32
33
34
35
36
37
38
39
40
41
42
43
44
45
46
47
48
49
50
51
52
53
54
55
56
57
58
59
60

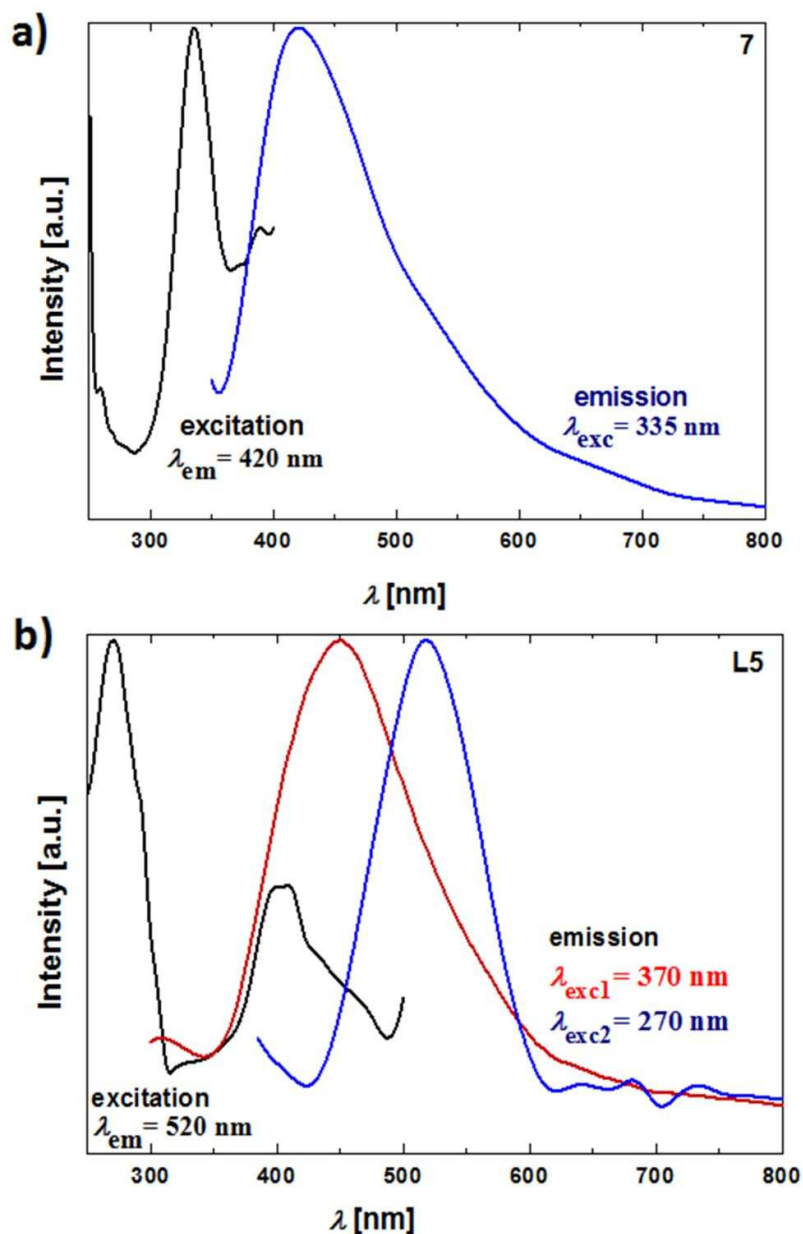


Figure 14. a) Solid-state photoluminescence of **7** and b) the free ligand **L5** presented through emission spectra for the indicated excitation wavelengths and excitation spectra for the indicated monitored emission wavelengths. All spectra were gathered at 77 K.

The UV-light-induced visible photoluminescence is also observed for $\{\text{Hg}(\text{II})_2\}$ dinuclear molecules of **10** (Figure 15). The distinct emission signal was detected under the deep UV light irradiation at $\lambda = 275$ nm which results in the broad emission band ranging from ca. $\lambda = 350$ to 600 nm, with the maximum in the blue region of the

1
2
3 spectrum, at $\lambda = 455$ nm. Similarly to **7**, the emission of **10** is also hypsochromically
4 shifted when compared with the free ligand **L6** exhibiting the green
5 photoluminescence with the broad emission band centered at $\lambda = 530$ nm (Table S6).
6 The related xy CIE 1931 chromaticity parameters change from yellowish green
7 (0.331, 0.445) for the free ligand to blue (0.219, 0.241) (Figure S1, Table S6). The
8 ligand **L6** contains only a single aromatic group of 1,2,4-triazole substituted with long
9 aliphatic tail involving thiourea-ethyl(acetate) moiety (Scheme 2), and its crystal
10 packing does not suggest the formation of any specific supramolecular aggregates
11 (Figure 4). The ILCT or LLCT emissive states are, then, rather excluded, and the
12 observed emission of **L6** can be assigned to the LC fluorescence. Both the excitation
13 as well as the emission patterns are shifted going from free ligand **L6** to **10** which
14 indicates the blue-shifted emission of a similar LC fluorescent origin. The blue-shift
15 can be explained by the significant molecular re-orientation of **L6** molecules upon
16 metal coordination in **10** (Figure 15). There is a lack of ligand-based supramolecular
17 stacks within the crystal structure of **10** which could have suggested the appearance
18 of some additional emissive LLCT states. However, the other possible sources of
19 emission in **10**, including the charge transfer states between iodide ion and Hg(II)
20 centers (halide-to-metal charge transfer, XMCT), between iodide and ligand **L6**
21 (halide-to-ligand charge transfer, XLCT) or between ligand **L6** and Hg(II) centers
22 (ligand-to-metal charge transfer, LMCT), cannot be easily excluded, as all are
23 accessible for the family of Hg(II) halides with aromatic heterocyclic ligands.^{34,46,47}

24
25
26
27
28
29
30
31
32
33
34
35
36
37
38 The clarification of the emission origin in **10**, is also provided by the theoretical
39 calculations of the electronic densities of states (Figure 19b, see next section). The
40 highest occupied states are of a predominant ligand character, in particular, the S
41 atoms of ligand **L6** contribute the most to these states. On the contrary, the lowest
42 unoccupied states are of the mixed **L6** and Hg(II) character, indicating that the lowest
43 energy optical transitions can be mainly described as the combination of LC and
44 LMCT (**L6** to Hg(II)) transitions. Therefore, the emission of **10** can be assigned to the
45 combined contributions from LC and LMCT transitions which agrees well with the
46 observed broad emission patterns visibly consisting of a few overlapping components
47 at ca. $\lambda = 380$, 450 and 530 nm, even with the tail towards higher wavelengths
48 (Figure 15). One additional remark should be given to the role of iodide ions which
49 bridges two Hg(II) centers within the dinuclear molecules of **10** (Figure 12). In the
50
51
52
53
54
55
56
57
58
59
60

1
2
3 calculated DOS, there is a significant contribution from iodide ions in the energy
4 states very near to the highest occupied states suggesting that there should be also
5 a non-zero contribution from the halide-related XMCT/XLCT states to the overall
6 emission. This interpretation becomes even more probable when noticing that the
7 analogous isostructural compounds **8** and **9**, containing chloride and bromide ions,
8 respectively, do not exhibit the emission even at 77 K. The calculated DOS of **8**
9 (Figure S13) indicates that the characters of lowest unoccupied, as well as highest
10 occupied states, remain similar in comparison to **10** (Figure 19b, see next section).
11 However, the contribution of chloride-related states is positioned well below the
12 highest occupied state which reveals almost a purely ligand-based character.
13 Besides, the lowest unoccupied states in **8**, which are still of a mixed Hg/L6
14 character, are split into two distinct parts. These modifications are expected to play
15 an important role in the observed experimental differences, the lack of detectable
16 emission in **8** and **9**, while the presence of distinct emission signal in **10**.
17
18
19
20
21
22
23
24
25
26
27
28
29
30
31
32
33
34
35
36
37
38
39
40
41
42
43
44
45
46
47
48
49
50
51
52
53
54
55
56
57
58
59
60

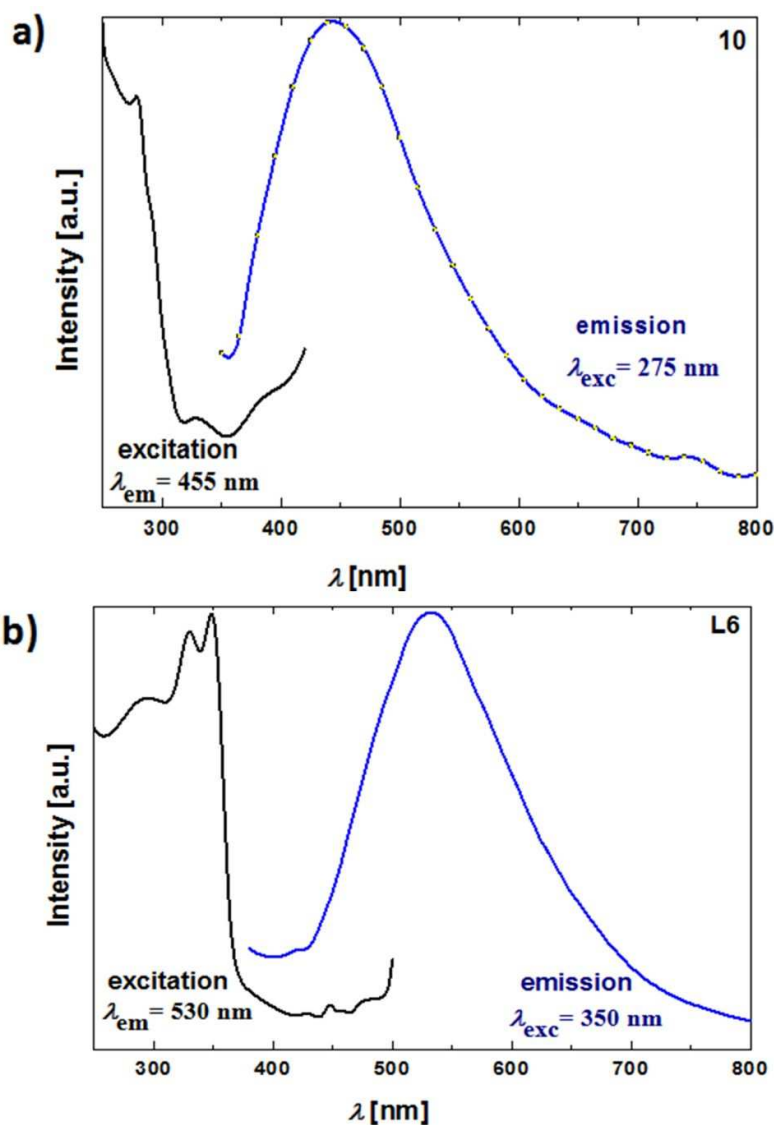


Figure 15. a) Solid-state photoluminescence of **10** and b) the free ligand **L6** presented through emission spectra for the indicated excitation wavelengths and excitation spectra for the indicated monitored emission wavelengths. All spectra were gathered at 77 K.

Visible light emission is also observed for compound **11** (Figure 16). Under UV-to-blue light excitation, it reveals an emission band centered at ca. $\lambda = 540$ nm which results in the green photoluminescence characterized by the (0.296, 0.550) xy CIE 1931 chromaticity parameters. This is the noticeably lower energy emission in comparison to the other investigated compounds **7** and **10** (Table S6), despite that the similar structure of the organic ligand, **L5'**, which is spontaneously formed from

1
2
3 ligand **L5** undergoes cyclization during the crystallization process (Scheme S1). This
4 ligand is only observed in the crystal structure of **11**, and could not be isolated
5 separately. Thus, its emission properties could not be determined. However, similarly
6 to other investigated ligands, it consists of the aromatic 1,2,4-triazole group with the
7 4-position substituent composed of an aliphatic ring with an additional thiocarbonyl
8 group. Due to the lack of a large π -conjugated system, this ligand is not expected to
9 exhibit any IL-charge-transfer transitions. In the crystal structure of **11**, there are no
10 specific supramolecular aggregates of the ligand which could lead to the related
11 LLCT emission. Therefore, the observed emission in **11** can be either the result of the
12 LC fluorescence or the CT emission involving Hg(II) metal centers and organic ligand
13 (LMCT). Alternatively, the CT emission related to the presence of iodide anions
14 coordinated to Hg(II) centers, being also in the proximity of organic ligands (possible
15 XMCT and XLCT states) could also be considered. The indication, on which emission
16 pathway is realized in compound **11**, is given by the theoretical calculations of the
17 electronic densities of states (Figure 19b, see next section). The highest occupied
18 state was found to be mostly of a halide character which is very different from results
19 found for compounds **7** and **10** (see above). On the contrary, the lowest unoccupied
20 state is strongly mixed, having both large contributions from Hg(II) metal centers
21 (predominant one) as well as organic ligands focused mainly on the C/N-based rings
22 rather than S atoms. As a result, the lowest energy optical transition is of XMCT and
23 XLCT characters. This indicates the XMCT/XLCT origin of the emission property in
24 **11** differs significantly compared to previously discussed **7** and **10** where LC and
25 LMCT emissive transitions dominated. A similar XLCT emission was reported for the
26 related Hg(II)-based complexes involving the simultaneous coordination of bromide
27 anions and other triazole-containing ligands, *N*-(1,2,4-triazol-4-yl)pyridine-3-
28 carboxamide.³⁴ In that case, similarly to **11**, the resulting emission appearing thanks
29 to the appropriate supramolecular arrangement of halide ions in close vicinity of
30 triazole-based ligands accompanying the direct coordination to Hg(II) centers.
31 Besides, it seems that such XLCT/XMCT transitions can produce a longer
32 wavelength emission in comparison to the LC/LMCT emissive state found in **7** and
33 **10**.

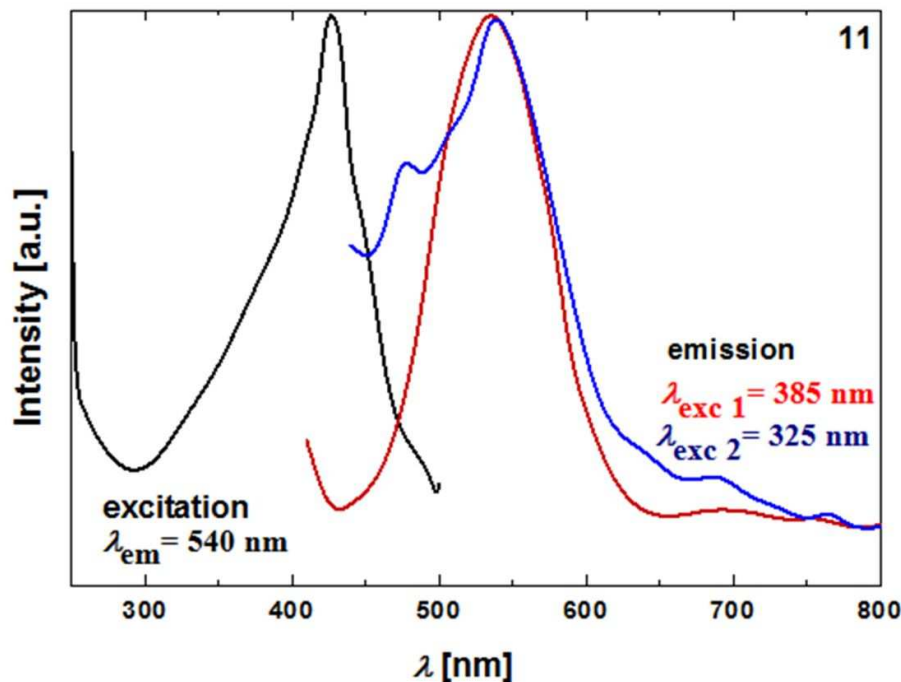


Figure 16. Solid-state photoluminescence of **11** presented through emission spectra for the indicated excitation wavelengths and excitation spectrum for the indicated monitored emission wavelength. All spectra were gathered at 77 K.

DISCUSSION

The conformation of the ligand is, naturally, one of the important factors which affect the crystal structure of a complex, but the nature of the central metal ions, and counter anions are rather the decision making factors for the conformation of ligands in coordination compounds.^{70,71} This has been shown in many case, wherein the conformation of both the free ligand (before reacting with metal ion) and the coordination compound (of the same ligand) showed differences.^{72,73} Interestingly, flexible ligands which have various plausible conformations are the key factor for successful self-assembly of important supramolecular compounds such as polycatenanes,⁷⁴ helices,^{75,76} braids,⁷⁷ Borromean rings,⁷⁸ 2D square grids,⁵ single walled metal-organic nanotube,⁶ and so on. However, it is a difficult task to predict the crystal structure of a coordination compound built from a flexible ligand, due to: i) various possible conformations and coordination modes of these ligands. ii) the difficulty to precisely determine their energies. iii) the kinetic and thermodynamic factors for the stability of the complexes and the crystal packing effect. In order to understand and precisely determine the final topological structure of the CPs, often

1
2
3 the molecular level building block approach or a crystal engineering approach is
4 used, in which the building blocks [supramolecular synthons^{79,80}/secondary building
5 units (SBU)^{81,82}] are capable of making predictable motifs within the resultant crystal
6 structure.
7
8

9
10 In this work, we designed and synthesize a series of new ligands based on a thiourea
11 backbone with 1,2,4 triazole functional groups on one side and alkyl, allyl or ester
12 functional groups on the other side, namely **L1-L6**) as well as a polymorph of **L4** and
13 a MeOH solvate of **L6** (Scheme 2). The ligand exhibits a degree of free rotation
14 around the N–N bond connecting the 1,2,4–triazole and thiourea moieties (N_{1,2,4}-
15 triazole–N_{thiourea}), and four extreme conformers can be generated by rotation around the
16 C–N bonds within the thiourea fragment, denoted as *syn–anti*, *syn–syn*, *anti–syn*, and
17 *anti–anti* (Scheme 3).
18
19
20
21
22

23 All ligand structures crystallize in centrosymmetric space groups forming a hydrogen
24 bonded homosynthon over the inversion center. In **L2**, **L3** and **L4**, this R₂²(8) ring
25 structure is formed between the NH adjacent to the triazole moiety and the thiourea
26 sulfur. All ligands are found in the syn-anti conformation (Scheme 4). **L1** and **L5** also
27 form a similar R₂²(8) ring structure, yet involving the other thiourea NH and with the
28 ligands in the anti-syn configuration. For **L1**, this situation results from the interaction
29 with the lattice water molecule, whereas for **L5** this is the result of packing
30 interactions, which fit very well with theoretical calculations showing that relative
31 energies between the different conformations is quite small (see next section). In **L6**,
32 a bifurcated hydrogen bond engaged in an intra- and inter-molecular interaction with
33 the carbonyl oxygen of the ester group is observed rather than thiocarbonyl. This also
34 imposes the anti-syn configuration. In all structures, the 1,2,4-triazole group is
35 oriented almost perpendicular (83.35° - 86.16°) to the thiourea (Figure 17).
36
37
38
39
40
41
42
43
44
45
46
47
48
49
50
51
52
53
54
55
56
57
58
59
60

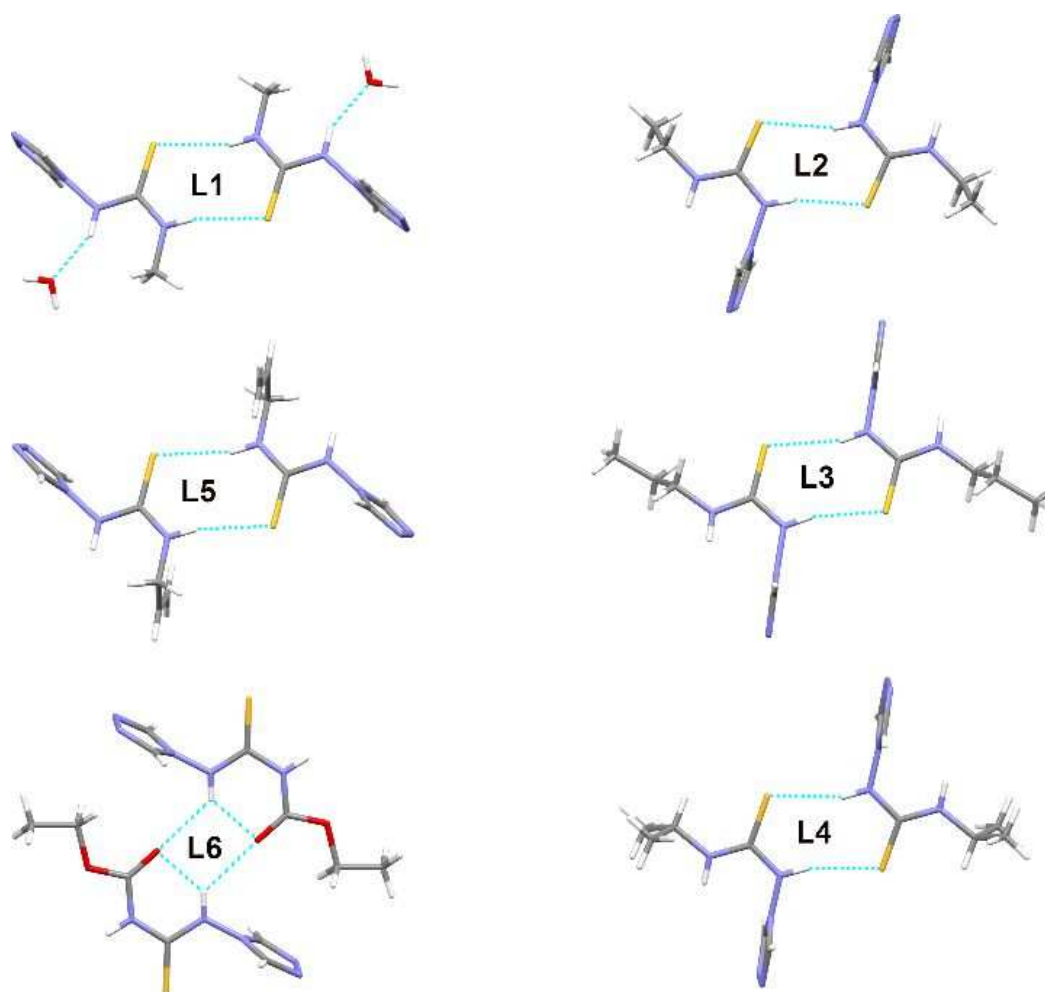


Figure 17. Stick representation of the homosynthons formed in L1-L6.

Although metal complexes with thiourea moieties are not uncommon (>1300 crystal structures recorded in the CSD,⁴² only 64 complexes involve a mercury complex, even less complexes (>50) are reported between mercury and a triazole ring. Moreover, only two ligands with the 1,2,4-triazole group directly attached to the thiourea moiety *via* an N-N bond are known,⁵⁵ and none as metal complex.

In all of our complexes, complexation with the Hg(II) atom occurs through the thiourea sulfur, with an offset angle Hg...S=C of 102.6° on average (range 96.6° – 109.9°), which is consistent with the CSD database (average 101.6° ±5.6). The 1,2,4-triazole moiety is in general found on opposite sides of the triazole sulfur to minimize repulsion (*syn-anti*, Scheme 2); nevertheless, the different conformations are very close in energy (see next section) and can easily convert into each other. Upon

1
2
3 deprotonation or proton transfer from the triazole NH to the triazole ring the other
4 configuration is observed (anti-syn or anti-anti, Scheme 2). Deprotonation allows
5 additional coordination through the triazole moiety and the formation of coordination
6 polymers, as observed for instance in **4** and **7**. The syn-syn configuration is not
7 observed amongst the current series. Deprotonation or proton transfer also
8 influences the coordination mode of the Hg center. A striking example is the
9 difference between complex **5** and **6**, both built from ligands **L4**. In **6**, charge
10 neutrality is achieved by two iodine anions, forming a tetrahedrally coordinated
11 binuclear complex, while in **5** only one chlorine anion is necessary, resulting in a
12 trigonal complex. It is as yet unclear how the deprotonation of the ligands is achieved
13 as all complexes were produced in similar manner by mixing the starting salt and
14 ligand in equimolar ratio and crystallizing the complexes by either evaporation or
15 convection, without any method systematically leading to deprotonation.
16
17
18
19
20
21
22
23

24 In Figure 18, the ligands in their free form and complexed to mercury are superposed
25 by fitting the thiourea moieties onto each other, which also demonstrates why the
26 syn-syn configuration is not observed as this would bring the triazole and alkyl ends
27 too close to each other. More details about the coordination modes of the ligands and
28 the corresponding bond lengths in compounds **1** to **10** are shown in Table S3. The
29 alkyl end of the ligand has little influence on the coordination mode or type of the
30 formed complexes, not even for ligand **L6**, where the free ligand shows inter and intra
31 molecular hydrogen bonding through the carbonyl oxygen.
32
33
34
35
36
37
38
39
40
41
42
43
44
45
46
47
48
49
50
51
52
53
54
55
56
57
58
59
60

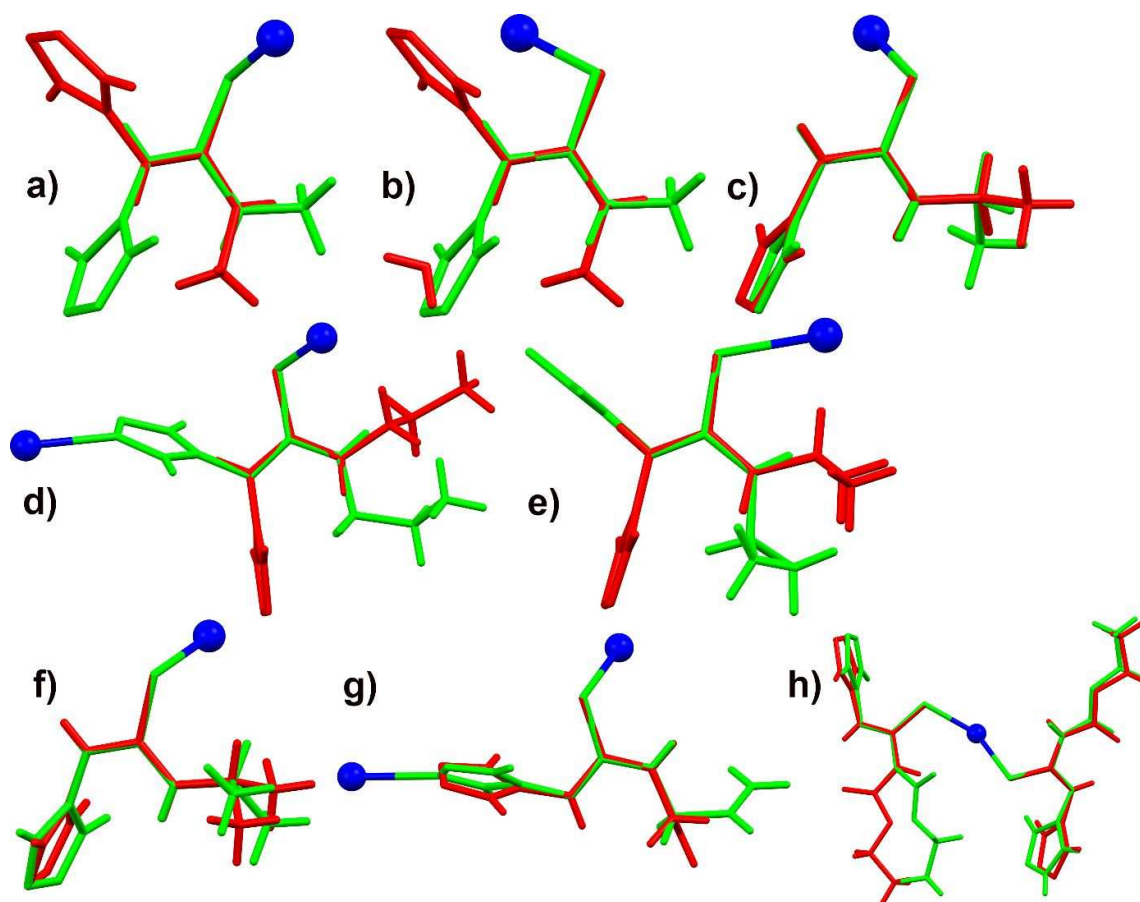


Figure 18. Overlay of ligand conformations as observed in the corresponding complexes (shown in green color with Hg atom as blue color) and free ligand (shown in red color) – a) **L1** and **1**; b) **L1** and **2** (the water molecule in the free ligand is also shown); c) **L2** and **3**; d) **L3** and **4** ; e) **L4** and **5**; f) **L4** and **6**; g) **L5** and **7**; h) **L6** and **8** (superposition of **L6** on both the neutral and deprotonated ligand of **8** are shown).

To investigate the influence of the ligand conformation, the relative stabilities of four different conformations of **L1**, **L4**, and **L6** as depicted in Scheme 2 were calculated by DFT, considering solvation effects from dichloromethane within the scope of a continuum solvation approximation (Figure 19a). It can be seen that, overall, all conformations of **L1** and **L4** have competitive stabilities, all lying within a 3 kcal/mol range. In the case of **L1** (anti-syn), the strength of, as an example, the nearest-neighbor triazole...H₂O interaction is computed to be -7.7 kcal/mol; this corroborates that the collection of intermolecular interactions in a given crystal can ‘override’ the small stability differences between the free-ligand conformers. **L6**, on the other hand, stands out because of its particularly stable anti-syn conformation; this preference

1
2
3 comes from the ability to create an intramolecular hydrogen bond between the
4 thiourea N-H and carbonyl C=O groups. In the case of **L6**, the (most stable) anti-syn
5 conformation is that which appears in the **L6** crystal structure. When the thiourea N-
6 H proton of **L6** is moved to the 1,2,4-triazole ring (labelled **L6'**), the strong
7 conformational preference for anti-syn is lost, because of the lack of an
8 intramolecular hydrogen bond, and the **L6'** anti-anti conformation becomes
9 competitive; the anti-anti and anti-syn conformations are the two conformers which
10 are adopted in the structures **8-10**. Thus, in the complexes **8-10**, the preferred
11 conformers of the free ligand are also arguably preserved. As is discussed below, for
12 every functional group (including **L6**) the scale of the intermolecular interactions is
13 much larger than the energy differences between conformers, but the set of ligands
14 we chose successfully maps out a rich structural space in which the conformational
15 preferences of the ligand are sometimes preserved (in the case of **L6**, albeit with
16 deprotonation being a decisive factor in the CP structures) and sometimes
17 composition-dependent (in the cases of **L1** and **L4**).
18
19
20
21
22
23
24
25
26
27
28
29
30
31
32
33
34
35
36
37
38
39
40
41
42
43
44
45
46
47
48
49
50
51
52
53
54
55
56
57
58
59
60

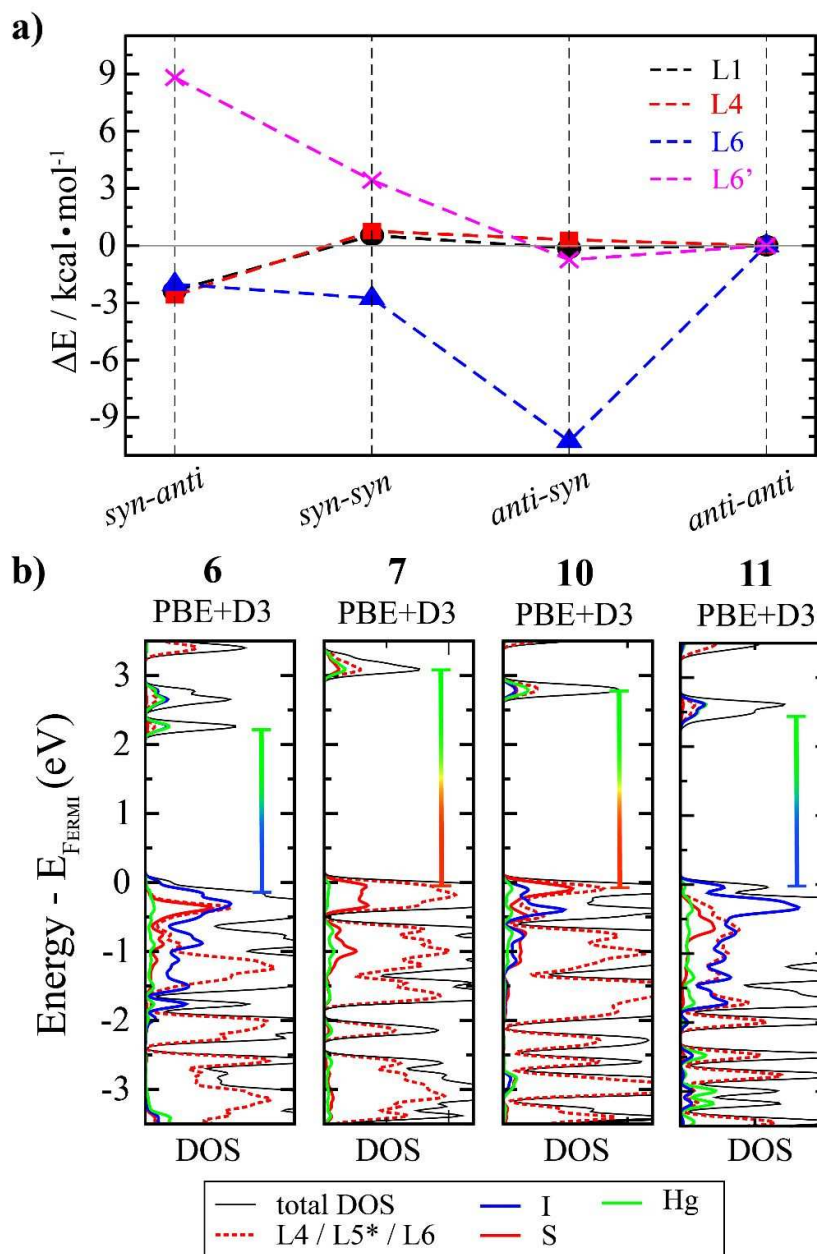


Figure 19. a) Relative total DFT energies of the ligand conformers defined in Scheme 2; shown are **L1**, **L4**, **L6**, and **L6'**, where **L6'** was built from **L6** by moving a proton from the thiourea subunit to the triazole subunit. b) Computed electronic densities of states (black line) for **6**, **7**, **10**, and **11** with the PBE+D3 functional; also shown, as indicated in the legend, are the atom-projected contributions to the total DOS, wherein the ligand contribution (i.e. **L4/L5/L6**) corresponds to the sum of all the atoms in the ligand. The Fermi energy is set to zero, and note that **11** does not contain **L5** (as described in the text).

1
2
3 One of the important factors which determine the supramolecular architectures
4 of coordination compounds is the presence of hydrogen bonding in the ligand
5 molecule. A design strategy based on the combination of both metal to ligand
6 coordination bonding and hydrogen bonding in designing various metal organic
7 supramolecular architectures, is an established area of research. Interestingly this
8 strategy attracted many materials chemists, due to the probability of structural
9 diversities, guest entrapment supported by hydrogen-bonding interactions, and
10 functional properties having potential applications. The important benefit of using
11 hydrogen bonding capable ligand for the synthesis of complexes is their ability to
12 form inter-chain or inter-network hydrogen bonding. The resulting materials show
13 intriguing supramolecular structure and robustness in their framework. Thiourea is a
14 well-known hydrogen bonding capable functionality, used in supramolecular
15 chemistry and coordination chemistry.^{83,84}

16
17
18
19
20
21
22
23
24
25 The ligands (**L1** to **L6**) contain hydrogen bonding capable functionalities such as
26 thiourea, 1,2,4-triazole, and alkyl, allyl or ester functional groups. More details of
27 hydrogen bonding of various functionalities of ligands, and solvent molecules are
28 shown in Table S2. The molecules of ligand **L1** in its free form, interact with each
29 other through lattice included water molecules, *via* N–H···O, N–H···S, O–H···N, and
30 C–H···S hydrogen bonding involving thiourea, triazole, and methyl moieties, resulting
31 in a 2D hydrogen bonded supramolecular network structure. Due to the *anti-syn*
32 conformation of ligand **L1**, thiourea···thiourea self–complimentary hydrogen bonding
33 (N–H···S) is absent in the crystal structure. On the other hand the N–H···N hydrogen
34 bonding (thiourea···triazole) in **1** resulted in a 3D network structure; **2** undergoes self–
35 assembly through thiourea···triazole hydrogen bonding (N–H···N) and π ··· π stacking
36 between the triazole rings, lead to the formation of a 1D hydrogen bonded chain
37 structure as the primary supramolecular structure, which further extended to a 2D
38 hydrogen bonded sheet through C–H···S and N–H···S hydrogen bonding involving
39 thiourea and lattice included DMSO molecules. Similar kind of supramolecular
40 structure is found in the crystal structure of **6**, the only difference is lattice included
41 solvent – DMSO in **2** and MeOH in **6**.

42
43
44
45
46
47
48
49
50
51
52
53 While ligand **L2** showed N–H···N and N–H···S hydrogen bonding involving the triazole
54 and thiourea which resulted in the formation of a 1D *zigzag* chain, **3** derived from **L2**

1
2
3 exhibit thiourea...triazole hydrogen bonding (N–H...N), and π ... π stacking interactions
4 (between triazole rings), resulted in 2D corrugated hydrogen bonded sheet structure,
5 which further self-assembled to 3D hydrogen bonded network with the support of N–
6 H...O hydrogen bonding involving lattice included MeOH with thiourea and triazole
7 moieties of the adjacent sheets. The ligands **L3** and **L4** also showed similar type of
8 hydrogen bonding and 1D *zigzag* chain structure like **L2**. The 2D square grid **4** built
9 from **L3**, having corrugated sheet like architecture, is stabilized by N–H...N
10 intramolecular hydrogen bonding interaction, and such sheets are further self-
11 assembled on top of each other with the support of weak van der Waals interactions.
12 Similar type of hydrogen bonding and packing is observed in **7**. However, the ligand
13 **L5** used for the synthesis of **7**, showed thiourea...triazole interaction through N–H...N
14 and N–H...S hydrogen bonding and lead to the formation of a 1D *zigzag* chain, which
15 is the primary supramolecular synthon. These chains are further assembled into 2D
16 hydrogen bonded corrugated sheet having a hexagonal grid topology via self-
17 complimentary thiourea...thiourea hydrogen bonding. **5** self-assembled to form a
18 macrocycle via N...N interaction between two triazole moieties. Moreover, other
19 supramolecular interactions such as C–H...Cl, C–H... π , π ... π stacking, involving
20 isopropyl C–H with metal bound Cl, triazole C–H with triazole ring, and thiourea C=S
21 with triazole ring, respectively, resulting in the formation of oval shaped microporous
22 supramolecular structure. However, the inclusion of MeOH molecules blocked such
23 pores. The self-assembly of isomorphous crystals of **8**, **9** and **10** through N–H...N
24 hydrogen bonding involving protonated form of triazole, thiourea and neutral triazole
25 functionalities, resulted in the formation of a 3D hydrogen bonded network structure.
26
27
28
29
30
31
32
33
34
35
36
37
38
39
40

41 In order to provide physical insight into factors contributing to the stability of the
42 reported species, extensive bonding analyses based on both cluster and periodic
43 calculations were performed (Figures S5-S13). We shall not discuss these data into
44 details, but provides herein only the most relevant findings. A more detailed
45 discussion is provided in the ESI. First of all, ETS-NOCV data have revealed, that
46 London dispersion forces are indispensable for the overall ligands stability – ΔE_{disp}
47 covers ~80% of the overall stabilization in **L4**, 68% in **L3** (CH...S, CH... π , CH...HC),
48 51% in **L1** (CH...S, π ... π), 48% in **L6** (σ -hole... π , NH...N), 42 % in **L5** (CH...N, CH... π)
49 and 38% in **L2** (CH... π), Figures S5-S10. As far as the corresponding metal polymers
50 are concerned, one shall state, that although dative-covalent [due to two ways
51
52
53
54
55
56
57
58
59
60

1
2
3 electrons transfer: $Lp(6s/5p, Hg) \rightarrow \sigma^*(S=C)$ and $Lp(S) \rightarrow \sigma^*(Hg-I/S)$] and
4 electrostatically dominated Hg–S bonds are quantitatively of prime importance, they
5 are supported by a bunch of unclassical mostly London dispersion driven non-
6 covalent interactions, including for example: $CH \cdots \pi$, $\pi \cdots \pi$, $CH \cdots I$ and $CH \cdots HC$ (Figure
7 S13); particularly the latter ones are intriguing and recently under extensive debates
8 due to real understanding of steric-crowding in small and sizable species⁸⁵⁻⁸⁸ (Figures
9 S12-S13). The varying motifs that are observed as a result of the self-assemblies in
10 **1-11** also result, as could be expected, in distinct valence and conduction band
11 electronic structures, as demonstrated in Figure 19b with **6**, **7**, **10**, and **11**. The
12 colored bars indicate the atoms in the coordination sphere of Hg which dominantly
13 contribute to valence and conduction band energy levels, and they can be seen to
14 change in both atom-type and length. Also, the make-up of the highest occupied
15 energy levels varies considerably, progressing from halide-based in **6** to thiolate-
16 character in **10** and significant triazole-character in **7**. It should be noted that the
17 particulars of the electronic structure are sensitive the level of theory that is used (for
18 example, the use of hybrid DFT functionals or the inclusion of spin-orbit relativistic
19 effects), but the results clearly show that a broad distribution of self-assembled
20 building blocks and of electronic structures is successfully realized.
21
22
23
24
25
26
27
28
29
30
31

32 CONCLUSIONS

33
34
35 In this work, we have explored a series of novel triazole-thiourea based ligands **L1-**
36 **L6** and their coordination and hydrogen bonded self-assembly with Hg(II), which
37 resulted in two mononuclear complexes **1** and **5** and five binuclear complexes **2**, **6**, **8**,
38 **9**, **10**, and four coordination polymers **3**, **4**, **7**, **11**. The SXRD analysis of these
39 complexes, revealed that their coordination or hydrogen bonding dimensionality,
40 topology and supramolecular structure are completely depending on various
41 parameters such as conformation of ligands, counter anions, hydrogen bonding
42 present in the ligand, and supramolecular interactions. While the self-assembly of
43 triazole-thiourea ligands having the substituents methyl, allyl, and ethyl ester such as
44 **L1**, **L5** and **L6**, respectively showed 2D hydrogen bonded corrugated sheet structure,
45 the triazole-thiourea ligands with ethyl, propyl and isopropyl moieties such as **L2**, **L3**
46 and **L4**, resulted in 1D *zigzag* hydrogen bonded chains. All of these ligands showed
47 thiourea \cdots thiourea ($N-H_{(TU)} \cdots S_{(TU)}$) hydrogen bonding, and also other supramolecular
48 interactions involving thiourea, triazole, and other functionalities. The ligands showed
49
50
51
52
53
54
55
56
57
58
59
60

1
2
3 *anti-syn* and *syn-anti* conformations, when it packed to 2D hydrogen bonded sheet
4 and 1D chains, respectively.
5

6
7 The supramolecular assembly of **1** with the support of thiourea⋯triazole (N–
8 H_(TU)⋯N_(TZ)) interaction leads to the formation of a 3D hydrogen bonded network
9 structure. The supramolecular structure of **2** is a 2D hydrogen bonded sheet
10 supported with thiourea⋯triazole, and thiourea⋯DMSO. Binuclear complex **6** also
11 has the same supramolecular structure as **2**, the only difference being the solvent of
12 crystallization. The self-assembly of mononuclear complex **5**, initially resulted in a
13 macrocycle, which further interacts each other to form a 1D hydrogen bonded chain
14 architecture, containing 'l' shaped subunits, sustained by N–H_(TZ)⋯N_(TZ). **8**, **9**, and **10**
15 are turn out to be isomorphous crystals, and self-assembled to a 3D hydrogen
16 bonded network structure supported by thiourea⋯thiourea (N–H_(TU)⋯S_(TU)),
17 triazole⋯triazole (N–H_(TZ)⋯N_(TZ)), and thiourea⋯triazole (N–H_(TU)⋯N_(TZ)). The 2D
18 square grid **4** and **7** undergo thiourea⋯triazole (N–H_(TU)⋯N_(TZ)) hydrogen bonding
19 interactions and resulted in the extension of the dimensionality from 2D CP to 3D
20 structure. The 1D CP **3**, extended its self-assembly to a 2D hydrogen bonded
21 corrugated sheet structure, with the support of various non-bonded interactions. 1D
22 zigzag CP **11** self-assembled with the support of various supramolecular interactions
23 and lead to the formation of a 3D hydrogen bonded network structure, embedding a
24 new ligand formed *in-situ*.
25
26
27
28
29
30
31
32
33
34
35
36

37 Among the series, **7**, **10**, and **11** were found to exhibit UV-light-induced
38 photoluminescence in the visible range. They show the great potential of mercury(II)-
39 halide coordination systems bearing 1,2,4-triazole derivatives in the generation of
40 multi-colored luminescence originating from remarkably diverse emissive electronic
41 states, ranging from ligand-centered fluorescence modified upon ligand coordination,
42 and combined with organic-ligand-to-metal charge transfer (**7** and **10**), as well as
43 halide-to-metal-charge transfer emission related to the d¹⁰ electronic configuration of
44 Hg(II), combined with the halide-to-ligand charge transfer taking advantage from the
45 appropriate arrangement of organic ligands and halide ions (**11**). The origin of the
46 emission transitions was elucidated on the basis of experimental observations
47 compared with the emission patterns of the respective organic ligands, with the
48 critical support of theoretical calculations of the electronic densities of states.
49 Interestingly, all emission effects were achieved in **7**, **10** and **11** by using relatively
50
51
52
53
54
55
56
57
58
59
60

1
2
3 small 1,2,4-triazole derivatives incorporating rather short substituents in comparison
4 to the previously reported Hg compounds with sterically expanded derivatives
5 bearing phenyl moieties giving the large π -conjugated systems and the related intra-
6 ligand or ligand-to-ligand charge transfer emissive states.²⁹ It indicates that the
7 reported Hg(II) halides incorporating flexible triazole-based ligands form a promising
8 class of luminescent molecular materials offering a remarkably rich diversity of
9 accessible and often co-existing emissive states which could be further explored
10 towards efficient dual emissive states for application in luminescent sensors or
11 ratiometric luminescent thermometers. This study is also important given that several
12 laboratories, including our team,⁸⁹ are currently designing hybrid materials including
13 such ligands to capture Hg from aquatic media. It will help these researchers to
14 understand the performances of their materials and improve their materials.
15
16
17
18
19
20
21
22
23
24
25
26
27
28
29
30
31
32
33
34
35
36
37
38
39
40
41
42
43
44
45
46
47
48
49
50
51
52
53
54
55
56
57
58
59
60

EXPERIMENTAL SECTION

Materials and Characterization Methods. All solvents were obtained from commercial sources. HgBr₂, HgI₂, Hg(NCS)₂, methyl thiocyanate, and allyl isothiocyanate were provided from Acros Organics. HgCl₂ and ethyl thiocyanate were obtained from Sigma Aldrich. Propyl isothiocyanate, isopropyl isothiocyanate and ethoxy carbonyl isothiocyanate were provided from TCI Chemicals. ¹H NMR spectra were recorded at 300 MHz on a Bruker AC300 instrument by using DMSO-d₆ solvent, with tetramethylsilane (TMS) as internal standard at ambient temperature. High Resolution mass spectral data were recorded in methanol on a Thermo Finnigan LCQ Ion Trap spectrometer in ESI mode, detecting positive ions. FT-IR spectra were recorded on Perkin Elmer 1310 spectrometer in the range 400-4000 cm⁻¹ using KBr pellets. CHN analyses were performed at MEDAC Ltd.

Diffuse reflectance spectra were obtained with a Perkin Elmer Lambda 9 UV/vis/NIR spectrophotometer equipped with a 60 mm integrating sphere and converted into absorption spectra by using the Kubelka–Munk function, using BaSO₄ as a reference. Powder X-ray diffraction patterns were recorded on a Siemens D5000 counter diffractometer working with a Cu K_α radiation ($\lambda = 1.5148 \text{ \AA}$) at 293 K. Photoluminescent characteristics, including solid-state emission and excitation spectra at room temperature as well as liquid nitrogen temperature, were investigated using an FS5 spectrofluorometer (Edinburgh Instruments) equipped with a Xe (150 W) arc lamp as an excitation source and a Hamamatsu photomultiplier of the R928P type as a detector. During these studies, the solid samples of ligands **L1–L6** as well as compounds **1–11** were measured in the form of a well-grinded powder placed at the bottom of a natural quartz tube which was inserted in the liquid nitrogen dewar mounted in the sample chamber of the spectrofluorometer. Background corrections were performed within the Fluoracle software (Edinburgh Instruments).

Syntheses

Synthesis of thiourea-triazole ligands **L1-L6**

Equimolar amounts of 4-amino-1,2,4-triazole and isothiocyanate derivatives were dissolved in ethanol (25 mL) in a 100 mL round bottom flask. The mixture was refluxed for 24 h at 60-75°C, resulting in a pale yellow clear solution. The solution was left to cool at room temperature and a white precipitate was collected by filtration. This product was washed with water (30 mL) and purified by recrystallization from methanol (20 mL) to obtain white crystals. The crystals were filtered, washed with ether, dried in air and kept in a desiccator over silica gel.

1-methyl-3-(4H-1,2,4-triazol-4-yl) thiourea (**L1**): Yield: (1.31 g) 75%. Mp: 208 °C. ¹H NMR (300 MHz, DMSO-d₆): δ 10.75 (br, s, 1H, NH), 8.68 (s, 2H CH of trz), 8.33 (br, s, 1H, NH), 2.82 (d, 3H of CH₃). Anal. Calc. for C₄H₇N₅S: C, 30.57.13; H, 4.49; N, 44.50 %; Found: C, 30.27; H, 4.36; N, 44.00%. IR (cm⁻¹) 3100, 1589, 1073, 614,755. MS (ESI): *m/z* 158.04959 [M+H]⁺.

1-ethyl-3-(4H-1,2,4-triazol-4-yl) thiourea (**L2**): Yield: (1.51 g) 74%. Mp.: 157 °C. ¹H NMR (300 MHz, DMSO-d₆): δ 10.63 (br, s, 1H, NH), 8.66 (s, 2H CH of trz), 8.45 (br, s, 1H, NH), 3.46 (m, 2H of CH₂), 1.11 (t, 3H of CH₃). IR (cm⁻¹) 3156, 2904, 1567, 1180, 1053, 743, 598. Elem. Anal. Calc. for C₄H₇N₅S: C, 34.90; H, 5.24; N, 41.39 %; Found: C, 35.07; H, 5.03; N, 40.90%. MS (ESI): *m/z* 172.06514 [M+H]⁺.

1-propyl-3-(4H-1,2,4-triazol-4-yl) thiourea (**L3**): Yield: (1.04 g) 47%. Mp: 159°C. ¹H NMR (300 MHz, DMSO-d₆): δ 10.59 (br, s, 1H, NH), 8.66 (s, 2H CH of trz), 8.48(br, s, 1H, NH), 3.42 (m, 2H of CH₂), 1.56 (sxt, 2H of CH₂), 0.86(t, 3H of CH₃). IR (cm⁻¹) 3112, 1572, 1179, 736, 600. Anal. Calc. for C₄H₇N₅S: C, 38.90; H, 5.99; N, 17.31 %. Found: C, 37.93; H, 5.97; N, 17.43%. MS (ESI): *m/z* 186.08079 [M+H]⁺.

1-isopropyl-3-(4H-1,2,4-triazol-4-yl) thiourea (**L4**): Yield (1.19 g) 54%. Mp: 162°C. ¹H NMR (300 MHz, DMSO-d₆): δ, 10.42 (br, s, 1H, NH), 8.63 (s, 2H CH of trz), 4.42 (br, s, 1H, NH), 4.39 (m, H, CH), 1.14 (d, 6H of 2 CH₃). IR (cm⁻¹): 3055, 1591, 1040,742, 631. Anal. Calc. for C₄H₇N₅S: C, 38.90; H, 5.97; N, 37.30 %. Found: C, 38.61; H, 5.99; N, 36.48%. MS (ESI): *m/z* 186.08079 [M+H]⁺.

1-allyl-3-(4H-1,2,4-triazol-4-yl) thiourea (**L5**): Yield: (1.42 g) 65%. Mp: 111 °C. ¹H NMR (300 MHz, DMSO-d₆): δ, 10.74 (s, 1H, NH), 8.68 (s, 2H CH of trz), 8.65 (br, s, 1H, NH), 5.84 (d, d, 1H of CH), 5.79 (m, 2H of CH₂), 4.10 (br, s, 2H, CH₂). FT-IR (cm⁻¹) 3230, 3083, 1350, 1540, 1230, 1080, 588. Anal. Calc. for C₄H₇N₅S: C, 39.33; H,

1
2
3 4.72; N, 38.22 %. Found: C, 38.22; H, 4.72; N, 38.02%. MS (ESI): m/z 184.06514
4 [M+H]⁺

5
6 Ethyl 2-(4H-1,2,4-triazol-4-yl) acetate thiourea (**L6**): Yield: (1.80 g) 70%. Mp: 169°C.
7
8 ¹H NMR (300 MHz, DMSO-*d*₆): δ , 12.22 (br, s, 1H, NH), 10.83 (br, s, 1H, NH), 8.65
9 (s, 2H CH of trz), 4.23 (m, 2H of CH₂), 1.29 (t, 3H of CH₃). IR (cm⁻¹) 3242, 1719, 1252,
10 1105. Anal. Calc. for C₄H₇N₅S: C, 33.48; H, 4.21; N, 32.54 %. Found: C, 33.03; H,
11 4.05; N, 32.12%. MS (ESI): m/z 216.05497 [M+H]⁺.
12
13
14

15
16 **L4-poly**: 0.136 mmol HgCl₂ (37 mg) and 0.27mmol of **L4** (50 mg) were dissolved in a
17 mixture of ethanol (6 mL) and THF (3mL). The mixture was stirred for 4h at room
18 temperature to yield to a turbid solution which was filtrated, yielding to a clear solution
19 which was left for slow evaporation. Plate of cubic colourless crystals were filtered off
20 after 4 days, washed with ethanol (3 mL) and dried under vacuum and transferred
21 into brown bottles to prevent from light exposure Yield: (42 mg) 83%. Mp~160°C. ¹H
22 NMR (300 MHz, DMSO-*d*₆): δ , 10.41 (br, s, 1H, NH), 8.63 (s, 2H CH of trz), 8.42 (br,
23 s, 1H, NH), 4.39 (t, 1H, CH), 3.47 (q, 2H CH₂ of Ethanol) 1.13 (d, 6H of 2 CH₃). 1.06
24 (d, 3H CH₃ of Ethanol). IR (cm⁻¹): 3094, 1570, 1062,746, 616.
25
26
27
28
29
30
31

32
33 **L6_MeOH-1**: 0.23 mmol 74 mg of Hg(NCS)₂ and 0.23 mmol of **L6** (50 mg) were
34 dissolved in a mixture of methanol (6 mL) and THF (3mL). The mixture was stirred for
35 4h at room temperature to yield to a turbid solution which was filtrated, yielding to a
36 clear solution which was left for slow evaporation. Plate of cubic colourless crystals
37 were filtered off after 4 days, washed with methanol (3 mL) and dried under vacuum
38 and transferred into brown bottles to prevent from light exposure. Yield: (26 mg) 52%.
39 Mp~ 170°C. ¹H NMR (300 MHz, DMSO-*d*₆): δ , 11.81 (br, s, 1H, NH), 10.83 (br, s, 1H,
40 NH), 8.65 (s, 2H CH of trz), 4.22 (q, 2H of CH₂), 1.27 (t, 3H of CH₃). IR (cm⁻¹) 3242,
41 1719, 1252, 1105.
42
43
44
45
46
47

48 **L6_MeOH-2**: 0.23 mmol of HgI₂ (105 mg) and 0.23 mmol of **L6** (50 mg) were placed
49 in the main arm of a *I* glass tube (Figure S7) which was filled with methanol. While
50 the main arm was heated in an oil bath at 60 °C, colorless block-shaped crystals
51 deposited on the cooler arm after 6 days. These were filtered off, washed with
52 methanol (3 mL) and dried in air. Yield: (35mg) 70.5%. Mp~ 168°C. ¹H NMR (300
53
54
55
56
57
58
59
60

MHz, DMSO- d_6): δ , 11.81 (br, s, 1H, NH), 8.65 (s, 2H CH of trz), 4.26 (q, 2H of CH₂), 1.27 (t, 3H of CH₃). IR (cm⁻¹) 3242, 1719, 1252, 1105.

Single crystals of **L6** were obtained as follows: 0.51 mmol of HgCl₂ (140 mg) and 0.26 mmol of **L6** (50 mg) were placed in the main arm of a Γ glass tube which was filled with methanol. While the main arm was heated in an oil bath at 60 °C, colorless block-shaped crystals deposited on the cooler arm after 3 days. These were filtered off, washed with methanol (3 mL) and dried in air. Yield: (40 mg) 71 %. Mp~ 166°C. ¹H NMR (300 MHz, DMSO- d_6): δ , 11.82 (br, s, 1H, NH), 8.65 (s, 2H CH of trz), 4.26 (q, 2H of CH₂), 1.26 (t, 3H of CH₃). IR (cm⁻¹) 3325, 1819, 1650, 1436, 1205, 650.

Synthesis of coordination compounds

[Hg(**L1**)₂(**L1**⁻)₂] (**1**): 0.32 mmol of **L1** (50 mg) and 0.1 mmol of Hg(NCS)₂ (34 mg) were placed in the main arm of a Γ glass tube which was filled with methanol. While the main arm was heated in an oil bath at 60 °C, colorless block-shaped crystals deposited on the cooler arm after 12 days. These were filtered off, washed with methanol (3 mL) and dried under vacuum. Yield: (81 mg) 32%. Crystals color changed to black when exposed to air and light after 4 days. Anal. Calc. for 1·4MeOH·10H₂O (HgC₂₀H₆₀N₂₀O₁₄S₄): C, 21.19; H, 5.33; N, 24.71 %; Found: C, 20.94; H, 2.66; N, 24.68 %. IR (KBr, cm⁻¹): 3300, 3145, 2800, 1630, 1500, 1420, 1350, 800.

{[(Hg)₂(**L1**)₂(μ_2 -I)₂(I)₂]·DMSO} (**2**): 0.23 mmol HgI₂ (106 mg) and 0.31 mmol **L1** (50 mg) were dissolved in a mixture of methanol (6 mL) and DMSO (2 mL). The mixture was stirred for 4h at room temperature to yield to a turbid solution which was filtrated, yielding to a clear solution which was left for slow evaporation. Colorless block-shaped crystals which were obtained after 8 days, were filtered off, washed with methanol (3 mL) and dried in air. Yield: (133 mg) 41%. Anal. Calc. for **2** (C₁₂H₂₆Hg₂I₄N₁₀O₂S₄): C, 10.45; H, 1.90; N, 10.15 %; Found: C, 9.93; H, 1.98; N, 10.08 %. IR (KBr, cm⁻¹): 3240, 3010, 2850, 2900, 1622, 1550, 1350, 1260, 830.

{[HgI(**L2**)(μ_2 -I)]·MeOH} _{∞} (**3**): 0.32 mmol of HgI₂ (147.5 mg) and 0.29 mmol of **L2** (50 mg) were dissolved in a mixture of methanol (6 mL) and THF (3mL). The mixture was stirred for 4h at room temperature to yield to a turbid solution which was filtrated, yielding to a clear solution which was left for slow evaporation. Yellow plate crystals

1
2
3 which were obtained after 13 days, were filtered off, washed with methanol (3 mL)
4 and dried in air. Yield: (92mg) 48%. Anal. Calc. for **3**·MeOH (C₇H₁₇HgI₂N₅O₂S): C,
5 12.19; H, 2.48; N, 10.15 %; Found: C, 11.74; H, 2.25; N, 10.12%. IR (KBr, cm⁻¹):
6 3200, 3000, 2820, 1630, 1550, 1470, 1360, 720.
7
8

9
10 $\{[(\text{Hg})_2(\mu\text{-L3}^-)_4]\}_\infty$ (**4**): 0.27 mmol of **L3** (50 mg) and 0.32 mmol of HgCl₂ (73 mg) were
11 placed in the main arm of a Γ glass tube which was filled with methanol. While the
12 main arm was heated in an oil bath at 60 °C, colorless block-shaped crystals
13 deposited on the cooler arm after two weeks. These were filtered off, washed with
14 methanol (3 mL) and dried in air vacuum. Yield: (53 mg) 17%. Anal. Calc. for **4**·6H₂O
15 (C₂₄H₄₈Hg₂N₂₀O₆S₄): C, 23.21; H, 3.89; N, 22.55 %; Found: C, 23.78; H, 3.89; N,
16 21.75%. IR (KBr, cm⁻¹): 3100, 3020, 2840, 1750, 1620, 1450, 1370, 1190, 890.
17
18
19
20
21

22 $\{[\text{HgCl}(\text{L4}^-)\text{L4}]\cdot\text{MeOH}\}$ (**5**): 0.27mmol HgCl₂ (74 mg) and 0.27mmol **L4** (50 mg) were
23 dissolved in a mixture of methanol (6 mL) and THF (3mL). The mixture was stirred for
24 4h at room temperature to yield to a turbid solution which was filtrated, yielding to a
25 clear solution which was left for slow evaporation. Plate colorless crystals were
26 filtered off after 8 days, washed with methanol (3 mL) and dried in air. Yield: (48 mg)
27 30%. Anal. Calc. for **5**·H₂O (C₁₃H₂₆ClHgN₁₀O₂S₂): C, 23.85; H, 4.00; N, 21.40%;
28 Found: C, 23.66; H, 3.48; N, 21.71%. IR (KBr, cm⁻¹): 3360, 3120, 2870, 1620, 1490,
29 1380, 1250, 870.
30
31
32
33
34

35 $\{[(\text{Hg})_2(\text{L4})_2(\mu_2\text{-I})_2(\text{I})_2]\cdot 2\text{MeOH}\}$ (**6**): 0.27 mmol of HgI₂ (123 mg) and 0.27 mmol of **L4**
36 (50 mg) were dissolved in a mixture of methanol (6 mL) and THF (3mL). The mixture
37 was stirred for 4h at room temperature to yield to a turbid solution which was filtrated,
38 yielding to a clear solution which was left for slow evaporation. Yellow block-shaped
39 crystals were filtered off after 4 days, washed with methanol (3 mL) and dried in air.
40 Yield: (115 mg) 32% Anal. Calc. for **6** (C₁₄H₃₀Hg₂I₄N₁₀O₂S₂): C, 12.52; H, 2.25; N,
41 10.43%; Found: C, 12.62; H, 2.14; N, 10.41%. IR (KBr, cm⁻¹): 3350, 3060, 2750,
42 1670, 1580, 1430, 1340, 980.
43
44
45
46
47
48

49 $\{[(\text{Hg})_2(\mu_2\text{-L5}^-)_4]\}_\infty$ (**7**): 0.27 mmol HgCl₂ (63 mg) and 0.27 mmol **L5** (50 mg) were
50 dissolved in a mixture of methanol (6 mL) and THF (3mL). The mixture was stirred for
51 4h at room temperature to yield to a turbid solution which was filtrated, yielding to a
52 clear solution which was left for slow evaporation. Colorless block-shaped crystals
53 were filtered off after 12 days, washed with methanol (3 mL) and dried under vacuum
54
55
56
57
58
59
60

1
2
3 and transferred into brown bottles to prevent from light exposure. Yield: (117 mg)
4 38%. Anal. Calc. for $7 \cdot 32\text{H}_2\text{O}$ ($\text{Hg}_2\text{C}_{24}\text{H}_{92}\text{N}_{20}\text{O}_{32}\text{S}_4$): C, 16.93; H, 5.45; N, 16.45 %;
5 Found: C, 16.55. H, 2.02, N 16.43%. IR (KBr, cm^{-1}): 3100, 3020, 1600, 2760, 1530,
6 1420, 1250, 740.
7
8

9
10 $[\text{Hg}_2(\mu_2\text{-Cl})_2(\text{L6}^-)_2(\text{L6})_2]$ (**8**): 0.39 mmol HgCl_2 (106 mg) and 0.23 mmol of **L6** (50 mg)
11 were dissolved in a mixture of methanol (6 mL) and THF (3mL). The mixture was
12 stirred for 4h at room temperature to yield to a turbid solution which was filtrated,
13 yielding to a clear solution which was left for slow evaporation. Plate colorless
14 crystals were filtered off after 10 days, washed with methanol (3 mL) and dried under
15 vacuum and transferred into brown bottles to prevent from light exposure. Yield: (91
16 mg) 36%. Anal. Calc. for $8 \cdot \text{MeOH}$ ($\text{C}_{25}\text{H}_{36}\text{Hg}_2\text{Cl}_2\text{N}_{20}\text{O}_9\text{S}_4$): C, 22.06; H, 2.67; N 20.58
17 %; Found C, 22.30; H, 2.70; N 20.88%. IR (KBr, cm^{-1}): 3220, 3040, 2560, 1500,
18 1480, 1345, 1280, 750.
19
20
21
22
23
24

25 $\{[\text{Hg}_2(\mu_2\text{-Br})_2(\text{L6}^-)_2(\text{L6})_2]\}$ (**9**): 0.23 mmol 84 mg of HgBr_2 and 0.23 mmol **L6** (50 mg)
26 were dissolved in a mixture of methanol (6 mL) and THF (3mL). The mixture was
27 stirred for 4h at room temperature to yield to a turbid solution which was filtrated,
28 yielding to a clear solution which was left for slow evaporation. Plate colorless
29 crystals were filtered off after 10 days, washed with methanol (3 mL) and dried under
30 vacuum and transferred into brown bottles to prevent from light exposure. Yield: (46
31 mg) 17%. Anal. Calc. for $9 \cdot 44\text{H}_2\text{O}$ ($\text{Hg}_2\text{C}_{22}\text{H}_{120}\text{N}_{20}\text{O}_{52}\text{Br}_2$): C, 13.04; H, 5.47; N, 12.67
32 %; Found: C, 13.56; H 2.38; N 11.93%. IR (KBr, cm^{-1}): 3210, 3035, 2620, 1560,
33 1480, 1330, 1270, 730.
34
35
36
37
38
39

40 $\{[\text{Hg}_2(\mu_2\text{-I})_2(\text{L6}^-)_2(\text{L6})_2]\}$ (**10**): 0.16 mmol of HgI_2 (74 mg) and 0.23 mmol of **L6** (50 mg)
41 were placed in the main arm of a Γ glass tube which was filled with methanol. While
42 the main arm was heated in an oil bath at 60 °C, colorless block-shaped crystals
43 deposited on the cooler arm after 12 days. These were filtered off, washed with
44 methanol (3 mL) and dried in air. Yield: (165 mg) 56%. Anal. Calc. for $10 \cdot 3\text{H}_2\text{O}$
45 ($\text{C}_{24}\text{H}_{38}\text{I}_2\text{Hg}_2\text{N}_{20}\text{O}_{11}\text{S}_4$): C, 18.41; H, 2.45; N, 17.89%; Found: C, 18.00; H, 2.18; N,
46 17.48%. IR (KBr, cm^{-1}): 3200, 3060, 1550, 1420, 1380, 1680, 810.
47
48
49
50
51
52
53
54
55
56
57
58
59
60

1
2
3 $\{[(\text{Hg})_2(\mu_3\text{-L5}')_3]\}_\infty$ (**11**): 0.29 mmol of HgI_2 (132 mg) and 0.27 mmol of **L5'** (50 mg)
4 were placed in the main arm of a Γ glass tube which was filled with methanol.
5
6 While the main arm was heated in an oil bath at 60 °C, colorless block-shaped
7 crystals deposited on the cooler arm after 13 days. These were filtered off, washed
8 with a methanol (3 mL) and dried in air. Yield: (82 mg) 32%. Anal. Calc. for **11**
9 $\text{C}_6\text{H}_8\text{I}_3\text{Hg}_2\text{N}_5\text{S}_4$: C, 7.34; H, 1.03; N, 7.13%; Found: C, 7.28; H, 1.18; N, 7.09%. IR
10 (KBr, cm^{-1}): 3100, 2650, 1620, 1420, 1370, 1210, 1170, 1010, 640.

14
15 **Single Crystals X-ray Diffraction.** Single crystal X-ray data of all compounds were
16 collected at room temperature with a MAR345 image plate using Mo $\text{K}\alpha$ ($\lambda = 0.71069$
17 Å) radiation. The crystals were selected from the mother solution, mounted in inert
18 oil, and for some transferred to the cold gas stream for flash cooling (**L1**, **L5**, **L6-**
19 **MeOH-1**, **8**). The unit cell parameters were refined using all the collected spots after
20 the integration process. The data were not corrected for absorption, but the data
21 collection mode partially takes the absorption phenomena into account. The
22 structures were solved by direct methods and refined by full-matrix least-squares on
23 F^2 using SHELXL97.^{90,91} All the non-hydrogen atoms were refined with anisotropic
24 temperature factors. All the H atoms were localized by Fourier difference and
25 included in the refinement with an isotropic temperature factor.

33
34 **Computational Details.** All calculations were performed using density functional
35 theory (DFT) methods within either the Vienna Ab-Initio Simulation Package
36 (VASP)⁹², for PBE+D3^{93,94} models of periodic networks, or the Amsterdam Density
37 Functional 2016 (ADF2016)^{95,96} programs, for BLYP+D3 models of molecules and
38 molecular clusters. Further details are given in the Supporting Information about the
39 computational parameters, results from selected periodic models with a hybrid DFT
40 functional and with spin-orbit relativistic effects, and an in-depth discussion about the
41 ligands' interaction energies.

47 ASSOCIATED CONTENT

50 Supporting Information

52 The Supporting information is available free of charge on the ACS Publication
53 website at DOI:xxxxxx.

55 Overview of NMR, Mass spectrometry, IR, UV-vis, luminescence, reaction
56 mechanism of **11**, crystallographic and theoretical modelling data (PDF)

Accession Codes

CCDC 2069121-2069129 and CCDC 2069131-2069142 contain the supplementary crystallographic data for this paper. These data can be obtained free of charge via www.ccdc.cam.ac.uk/data_request/cif, or by emailing data_request@ccdc.cam.ac.uk, or by contacting The Cambridge Crystallographic Data Centre, 12 Union Road, 718 Cambridge CB2 1EZ, UK; fax: +44 1223 336033.

AUTHOR INFORMATION

Corresponding Author

Yann Garcia – Institute of Condensed Matter and Nanosciences, Molecular Chemistry, Materials and Catalysis (IMCN/MOST), Université catholique de Louvain, 1348 Louvain-la-Neuve, Belgium; orcid.org/0000-0002-3105-0735; Email: yann.garcia@uclouvain.be

Notes

The authors declare no competing financial interest.

ACKNOWLEDGEMENTS

We acknowledge financial support from FNRS (CDR 33694457, PDR T.0095.21), Wallonie Bruxelles International (WBI COP22 Morocco, stipendium of excellence for H. B.), CNRST (ESRFC-CNRST-P10) as well as FNRS-PAN and WBI-MNiSW.

REFERENCES

- (1) Bladin, J. A. Ueber von Dicyanphenylhydrazin abgeleitete Verbindungen. *Chem. Ber.* **1885**, *18*, 1544.
- (2) Zhang, H-Z.; Damu, G. L. V.; Cai, G-X.; Zhou, C-H. Current Developments in the Syntheses of 1,2,4-Triazole Compounds. *Curr. Org. Chem.* **2014**, *18*, 359-406.
- (3) Thakur, A.; Gupta, P. S.; Shukla, P. K.; Verma, A.; Pathak, P. 1,2,4-Triazole Scaffolds: Recent Advances and Pharmacological Applications. *Int. J. Curr. Res. Aca. Rev.* **2016**, *4*, 27-296.
- (4) El Rayes, S. M. Convenient Synthesis and Antimicrobial Activity of Some Novel Amino Acid Coupled Triazoles. *Molecules.* **2010**, *15*, 6759-6772.

1
2
3 (5) Adarsh, N. N.; Dîrtu, M. M.; Guionneau, P.; Devlin, E.; Sanakis, Y.; Howard, J. A. K.;
4 Chattopadhyay, B.; Garcia, Y. One-Dimensional Looped Chain and Two-Dimensional Square
5 Grid Coordination Polymers: Encapsulation of Bis (1,2,4-Triazole)-*trans*-cyclohexane into the
6 Voids. *Eur. J. Inorg. Chem.* **2019**, 585-591.

7
8 (6) Adarsh, N. N.; Dîrtu, M. M.; Naik, A. D.; Leonard, A. F.; Campagnol, N.; Robeyns, K.;
9 Snauwaert, J.; Fransaer, J.; Su, B. L.; Garcia, Y. Single-walled metal-organic nanotube built
10 from a simple synthon. *Chem. Eur. J.* **2015**, 21, 4300–4307.

11
12 (7) Naik, A. D.; Dîrtu, M. M.; Leonard, A.; Tinant, B.; Marchand-Brynaert, J.; Su, B. L.; Garcia,
13 Y. Engineering Three-Dimensional Chains of Porous Nanoballs from a 1,2,4-Triazole-
14 carboxylate Supramolecular Synthon. *Cryst. Growth Des.* **2010**, 10, 1798–1807.

15
16 (8) Dîrtu, M. M.; Neuhausen, C.; Naik, A. D.; Leonard, A.; Robert, F.; Marchand-Brynaert, J.;
17 Su, B. L.; Garcia, Y. Superlative scaffold of 1,2,4-Triazole derivative of glycine steering linear
18 chain to a chiral helicate. *Cryst. Growth. Des.* **2011**, 11, 1375–1384.

19
20 (9) Naik, A. D.; Tinant, B.; Leonard, A.; Marchand-Brynaert, J.; Su, B-L.; Garcia, Y. (Di)-
21 aminoguanidine Functionalization through Transamination: An Avenue to an Auspicious
22 Class of Supramolecular Synthons. *Cryst. Growth Des.* **2011**, 11, 4034–4043.

23
24 (10) Naik, A. D.; Dîrtu, M. M.; Railliet, A. P.; Marchand-Brynaert, J.; Garcia, Y. Coordination
25 polymers and metal organic frameworks derived from 1,2,4-triazole amino acid linkers.
26 *Polymers.* **2011**, 3, 1750-1775.

27
28 (11) Kobalz, K.; Kobalz, M.; Möllmer, J.; Junghans, U.; Lange, M.; Bergmann, J.; Dietrich, S;
29 Wecks, M.; Gläser, R.; Krautscheid, H. Paddle Wheel Based Triazolyl Isophthalate MOFs:
30 Impact of Linker Modification on Crystal Structure and Gas Sorption Properties. *Inorg. Chem.*
31 **2016**, 55, 6938–6948.

32
33 (12) Dong, Y.; Peng, P.; Hu, B.; Su, H.; Li, S.; Pang, S. High-Density Energetic Metal–
34 Organic Frameworks Based on the 5,5'-Dinitro-2H,2'H-3,3'-bi-1,2,4-triazole. *Molecules.*
35 **2017**, 22, 1068.

36
37 (13) Liu, B.; Yang, T. Y.; Feng, H. J.; Zhang, Z. H.; Xu, L. A 3D chiral metal-organic
38 framework based on left-handed helices containing 3-amino-1 H-1,2,4-triazole ligand. *J.*
39 *Solid State Chem.* **2015**, 230, 90–94.

40
41 (14) Kitagawa, S; Kitaura, R.; Noro, S. I. Angew. Functional Porous Coordination *Polymers.*
42 *Chem. Int. Ed.* **2004**, 43, 2334–2375.

43
44 (15) Adarsh, N. N.; Novio, F.; Ruiz-Molina, D. Coordination polymers built from 1,4-
45 bis(imidazol-1-ylmethyl)benzene: from crystalline to amorphous. *Dalton Trans.* **2016**, 45,
46 11233-11255.

47
48 (16) Li, B.; Wen, H. M.; Zhou, W.; Chen, B. Porous Metal–Organic Frameworks for Gas
49 Storage and Separation: What, How, and Why? *J. Phys. Chem. Lett.* **2014**, 5, 3468–3479
50
51
52
53
54
55
56
57
58
59
60

- 1
2
3 (17) Li, H.; Wang, K.; Sun, Y.; Lollar, C. T.; Li, J.; Zhou, H. C. Recent advances in gas
4 storage and separation using metal–organic frameworks. *Mater. Today*. **2018**, *21*, 108-121.
5
6 (18) Li, J. R.; Sculley, J.; Zhou, H. C. Metal–Organic Frameworks for Separations. *Chem.*
7 *Rev.* **2012**, *112*, 869–932.
8
9 (19) Yu, X.; Wang, L.; Cohen, S. M. Photocatalytic metal–organic frameworks for organic
10 transformations. *CrystEngComm*. **2017**, *19*, 4126-4136.
11 (20) Paul, M.; Adarsh, N. N.; Dastidar, P. Secondary Building Unit (SBU) Controlled
12 Formation of a Catalytically Active Metal–Organic Polyhedron (MOP) Derived from a Flexible
13 Tripodal Ligand. *Cryst. Growth Des.* **2014**, *14*, 1331–1337.
14
15 (21) Garcia, Y.; Adarsh, N. N.; Naik, A. D. Crystal engineering of Fe(II) spin crossover
16 coordination polymers derived from triazole or tetrazole ligands. *Chimia* **2013**, *67*, 411–418.
17
18 (22) Suárez-García, S.; Adarsh, N. N.; Molnár, G.; Bousseksou, A.; Garcia, Y.; Dîrtu, M. M.;
19 Saiz-Poseu, J.; Robles, R.; Ordejón, P.; Ruiz-Molina, D. Spin-Crossover in an Exfoliated 2D
20 Coordination Polymer and Its Implementation in Thermochromic Films. *ACS Appl. Nano*
21 *Mater.* **2018**, *1*, 2662–2668.
22
23 (23) Adarsh, N. N.; Frias, C.; Lohidakshan, T. M.; Lorenzo, J.; Novio, F.; Garcia-Pardo, J.;
24 Ruiz-Molina, D. Pt(IV)-based nanoscale coordination polymers: Antitumor activity, cellular up
25 take and interactions with nuclear DNA. *Chem. Eng. J.* **2018**, *340*, 94-102.
26
27 (24) Lu, K.; Aung, T.; Guo, N.; Weichselbaum, R.; Lin, W. Nanoscale Metal–Organic
28 Frameworks for Therapeutic, Imaging, and Sensing Applications. *Adv. Mater.* **2018**, *30*,
29 707634.
30
31 (25) Guo, Y.; Xue, S.; Dîrtu, M. M.; Garcia, Y. A versatile iron(II)-based colorimetric sensor
32 for the vapor-phase detection of alcohols and toxic gases. *J. Mater. Chem. C.* **2018**, *6*, 3895-
33 3900.
34
35 (26) Naik, A. D.; Robeyns, K.; Meunier, C. F.; Léonard, A. F.; Rotaru, A.; Tinant, B.;
36 Filinchuk, Y.; Su, B. L.; Garcia, Y. Selective and reusable iron(II)-based molecular sensor for
37 the vapor-phase detection of alcohols. *Inorg. Chem.* **2014**, *55*, 1263–1265.
38
39 (27) Wang, W.; Li, J.-L.; Jiang, C.; Hu, P.; Li, B.; Zhang, T.; Zhou, H.-C. An efficient
40 strategy for improving the luminescent sensing performance of a terbium(III) metal–organic
41 framework towards multiple substances. *Chem. Commun.* **2018**, *54*, 13271–13274.
42
43 (28) Adarsh, N. N.; Dastidar, P. Coordination polymers: what has been achieved in going
44 from *innocent* 4,4'-bipyridine to bis-pyridyl ligands having a *non-innocent* backbone?
45 *Chem. Soc. Rev.* **2012**, *41*, 3039-3060.
46
47 (29) Wang, Z.; S. M. Cohen. Postsynthetic modification of metal–organic frameworks. *Chem.*
48 *Soc. Rev.* **2009**, *38*, 1315-1329.
49
50 (30) Tehrani, A. A.; Esrafil, L.; Abedi, S.; Morsali, A.; Carlucci, L.; Proserpio, D. M.; Wang, J.
51 Junk, P. C.; Liu, T. Urea Metal–Organic Frameworks for Nitro-Substituted Compounds
52 Sensing. *Inorg. Chem.* **2017**, *56*, 1446–1454.
53
54
55
56
57
58
59
60

1
2
3 (31) Wang, X-J.; Li, J.; Li, Q-Y.; Li, P-Z.; Lu, H.; Lao, Q.; Ni, R.; Shi, Y.; Zhao, Y. A urea
4 decorated (3,24)-connected *rht*-type metal–organic framework exhibiting high gas uptake
5 capability and catalytic activity. *CrystEngComm*. **2015**, *17*, 4632–4636.

6
7 (32) Chen, C.; Zhang, M.; Zhang, W.; Bai, J. Stable Amide-Functionalized Metal–Organic
8 Framework with Highly Selective CO₂ Adsorption. *Inorg. Chem*. **2019**, *58*, 2729–2735.

9
10 (33) Banerjee, S.; Kumar, D.P.; Bandyopadhyay, S.; Adarsh, N. N.; Dastidar, P. A New Series
11 of Cu^{II} Coordination Polymers Derived from Bis-pyridyl-bis-urea Ligands and Various
12 Dicarboxylates and Their Role in Methanolysis of Epoxide Ring-Opening Catalysis. *Cryst.*
13 *Growth Des.* **2012**, *12*, 5546–5554.

14
15 (34) Custelcean, R.; Sellin, V.; Moyer, B. A. Sulfate separation by selective crystallization of
16 a urea-functionalized metal–organic framework. *Chem. Commun.* **2007**, *15*, 1541–1543.

17
18 (35) Roberts, J. M.; Fini, B. M.; Sarjeant, A. A.; Farha, O. K.; Hupp, J. T.; Scheidt, K. A. Urea
19 metal-organic frameworks as effective and size-selective hydrogen-bond catalysts. *J. Am.*
20 *Chem. Soc.* **2012**, *134*, 3334–3337.

21
22 (36) Li, W.; Thirumurugan, A.; Barton, P. T.; Lin, Z.; Henke, S.; Yeung, H. H. M.; Wharmby,
23 M.T.; Bithel, E. G.; Howard, C. J.; Cheetham, A. K. Mechanical Tunability via Hydrogen
24 Bonding in Metal–Organic Frameworks with the Perovskite Architecture. *J. Am. Chem. Soc.*
25 **2014**, *136*, 7801–7804.

26
27 (37) Tan, K.; Jensen, S.; Zuluaga, S.; Chapman, E. K.; Wang, H.; Rahman, R.; Cure, J.; Kim,
28 T-H.; Li, J.; Thonhauser, T.; Chabal, Y. J. Role of Hydrogen Bonding on Transport of
29 Coadsorbed Gases in Metal–Organic Frameworks Materials. *J. Am. Chem. Soc.* **2018**, *140*,
30 856–859.

31
32 (38) Alegre-Requena, J. V.; Marqués-López, E.; Herrera, R. P.; Díaz, D. D. Metal–organic
33 frameworks (MOFs) bring new life to hydrogen-bonding organocatalysts in confined spaces.
34 *CrystEngComm*. **2016**, *18*, 3985–3995.

35
36 (39) Lu, H.; Zhu, Y.; Chen, N.; Gao, Y.; Guo, X.; Li, G. M. Tang Ligand-Directed Assembly of
37 a Series of Complexes Bearing Thiourea-Based Carboxylates. *Cryst. Growth Des.* **2011**, *11*,
38 5241–5252.

39
40 (40) Hollmann, K.; Oppermann, A.; Witte, M.; Li, S.; Amen, M.; Flörke, U.; Egold, H.; Henkel,
41 G.; Herres-Pawlis, S. Copper(I) Complexes with Thiourea Derivatives as Ligands: Revealing
42 Secrets of Their Bonding Scheme. *Eur. J. Inorg. Chem.* **2017**, 1266–1279.

43
44 (41) Hollmann, K.; Oppermann, A.; Amen, M.; Flörke, U.; Egold, H.; Hoffmann, A.; Herres-
45 Pawlis, S.; Henkel, G. Addressing Hydrogen Bonding Motifs by Suited Substitution of
46 Thioureas. *Anorg. Allg. Chem.* **2016**, *642*, 660–669.

47
48 (42) CSD, version 5.41, August **2020**.

49
50 (43) Babashkina, M. G.; Safin, D. A.; Robeyns, K.; Garcia, Y. Complexation properties of the
51 crown ether-containing *N*-thiophosphorylated thiourea towards Ni^{II}. *Dalton Trans.* **2012**, *41*,
52 1451–1453.

53
54 (44) Safin, D. A.; Babashkina, M. G.; Robeyns, K.; Garcia, Y. Halogen anion-induced
55 formation of [(PdLX)₂] (X=Cl⁻, Br⁻, I⁻) vs. [PdL₂] (L = [6 MeO(O)CC₆H₄NHC(S)NP(S)(OiPr)₂]-):
56
57
58
59
60

1
2
3 Reversible photoinduced cis/trans isomerization of [PdL₂]. *Dalton Trans.* **2012**, 41, 4324-
4 4327.

5 (45) Saeed, A.; Bolte, M.; Erben, M. F.; Pérez, H. Intermolecular interactions in crystalline 1-
6 (adamantane-1-carbonyl)-3-substituted thioureas with Hirshfeld surface analysis.
7 *CrystEngComm.* **2015**, 17, 7551-7563.

8
9
10 (46) Saeed, A.; Florke, U.; Erben, M. F. A review on the chemistry, coordination, structure
11 and biological properties of 1-(acyl/aroyl)-3-(substituted) thioureas. *J. Sulfur. Chem.* **2014**,
12 35, 318-355.

13
14
15 (47) Dîrtu, M. M.; Adarsh, N. N.; Naik, A. D.; Robeyns, K.; Garcia, Y. Supramolecular
16 homochiral helicity and zigzag hydrogen bonding networks in 1,2,4-triazole derived amino
17 ester and amino acid. *New J. Chem.* **2016**, 40, 9025-9029.

18
19
20 (48) Bowmaker, G. A.; Hanna, J.V.; Pakawatchai, C.; Skelton, B. W.; Thanyasirikul, Y.;
21 White, A. H. Crystal structures and vibrational spectroscopy of copper(I) thiourea complexes.
22 *Inorg. Chem.* **2009**, 48, 350-368.

23
24 (49) Casas, J. S.; García-Tasende, M. S.; Sordo, J. Cu(II) Benzoylpyridine
25 Thiosemicarbazone Complexes: Inhibition of Human Topoisomerase II α and Activity against
26 Breast Cancer Cells. *Coord. Chem. Rev.* **2000**, 209, 197-261.

27
28 (50) Liu, K.; Shi, W.; Cheng, P. The coordination chemistry of Zn(II), Cd(II) and Hg(II)
29 complexes with 1,2,4-triazole derivatives. *Dalton Trans.* **2011**, 40, 8475.

30
31 (51) Benaissa, H.; Wolff, M; Robeyns, K; Knor, G.; Van Hecke, K; Campagnol, N.; Fransaer,
32 J.; Garcia, Y. Syntheses, crystal structures, luminescent properties, and electrochemical
33 synthesis of group 12 element coordination polymers with 4-substituted-1,2,4-triazole
34 ligands. *Cryst.Growth Des.* **2019**, 19, 5292-5307

35
36 (52) Guo, X. F.; Qian, X. H.; Jia, L. H. A Highly Selective and Sensitive Fluorescent
37 Chemosensor for Hg²⁺ in Neutral Buffer Aqueous Solution. *J. Am. Chem. Soc.* **2004**, 126,
38 2272.

39
40 (53) Yu, Y.; Lin, L.-R.; Yang, K.-B.; Zhong, X.; Huang, R.-B.; Zheng, L.-S. *p*-
41 Dimethylaminobenzaldehyde thiosemicarbazone: A simple novel selective and sensitive
42 fluorescent sensor for mercury(II) in aqueous solution *Talanta* **2006**, 69, 103.

43
44 (54) Wang, L.; Zhu, X.- J.; Wong, W.-Y.; Guo, J.- P.; Wong, W.-K.; Li, Z.-Y. J.
45 Dipyrrrolylquinoxaline-bridged Schiff bases: a new class of fluorescent sensors for mercury(ii).
46 *Dalton Trans.* **2005**, 3235.

47
48 (55) Bielenica, A.; Kedzierska, E.; Fidecka, S.; Maluszynska, H.; Mirosław, B.; Koziol, A.E.;
49 Stefanska, J.; Madeddu, S.; Giliberti, G.; Sanna, G.; Struga, M. Synthesis, antimicrobial and
50 pharmacological evaluation of thiourea derivatives of 4H-1,2,4-triazole. *Lett. Drug. Discov.*
51 **2016**, 12, 263.

52
53 (56) Zhang, Y.-M.; Yang, Li-Zi.; Lin, Q.; We, T.-B. Synthesis and crystal structure of bis{(μ -
54 chloro)-chloro-[N-benzoyl-N'-(2-hydroxyethyl)thiourea]mercury(II)}. *J. Coord. Chem.* **2005**,
55 58, 1675-1679.

1
2
3 (57) Glaser, Rainer E. Organic Spectroscopy, Vibrational Spectroscopy Tutorial: Sulfur and
4 Phosphorus, Carissa Hampton Dustin Demoin Fall. **2010**.

5
6 (58) Samiei Paqhaleh, D. M.; Aminjanov, A. A.; Amani, V. Dimeric and polymeric mercury(II)
7 complexes containing 4-methyl-1,2,4-triazole-3-thiol ligand: X-ray studies, spectroscopic
8 characterization, and thermal analyses. *J. Inorg. Organomet. Polym Mater.* **2015**, *146*, 559–
9 569.

10
11 (59) Jiang, Y. L.; Wang, Y. L.; Lin, J. X.; Liu, Q. Y.; Lu, Z.H.; Zhang, N.; Wei, J. J.; Li, L.Q.
12 Syntheses, structures and properties of coordination polymers of cadmium(ii) with 4-methyl-
13 1,2,4-triazole-3-thiol ligand. *CrystEngComm.* **2011**, *13*, 1697-1706.

14
15 (60) Jolley, J.; Cross, W. I.; Pritchard, R. G.; McAuliffe, C. A.; Nolan, K. B. Synthesis and
16 characterisation of mercaptoimidazole, mercaptopyrimidine and mercaptopyridine complexes
17 of platinum(II) and platinum(III). The crystal and molecular structures of tetra(2-
18 mercaptobenzimidazole)- and tetra(2-mercaptoimidazole)platinum(II) chloride. *Inorg. Chim*
19 *Acta.* **2001**, *315*, 36-43.

20
21 (61) Bellamy, L. J. The infrared spectra of complex molecules, 3rd edn. *Chapman and Hall*,
22 *London.* **1975**.

23
24 (62) TOPOS 4.0, A Program Package for Multipurpose Crystallochemical Analysis, V. A.
25 Blatov, D. M. Proserpio. <http://www.topos.ssu.samara.ru/>.

26
27 (63) Blatov, V. A. "Multipurpose crystallochemical analysis with the program package
28 TOPOS," *IUCr Comp Comm Newsletter.* **2006**, *4*, 38.

29
30 (64) Addison, A. W.; Rao, T. N.; Reedjik, J.; van Rjin, J.; Verschoor, G. C. *J. Chem. Soc.,*
31 *Dalton Trans.* **1984**, 1349-1356.

32
33 (65) Khalaji, A. D.; Bahramian, B.; Jafari, K.; Fejfarova, K.; Dusek, M. *Russ. J Coord. Chem.*
34 **2013**, *39*, 877–884.

35
36 (66) Morsali, A.; Masoomi, M. Y. *Coord. Chem. Rev.* **2009**, *253*, 1882-1905.

37
38 (67) Volpi, G.; Priola, E.; Garino, C.; Daolio, A.; Rabezzana, R.; Benz, P.; Giordana, A.;
39 Diana, E.; Gobetto, R. Blue fluorescent zinc(II) complexes based on tunable imidazo[1,5-
40 a]pyridines. *Inorg. Chim. Acta.* **2020**, *509*, 119662.

41
42 (68) Cho, M.; Shin, H. J.; Kusumahastuti, D. K. A.; Yeo, H.; Min, K. S. Monomeric and
43 tetrameric mercury (II) complexes with iodo and N₂O₂/N₃O ligands: Structure and blue
44 luminescence. *Inorg. Chim. Acta.* **2020**, *511*, 119789.

45
46 (69) Liu, D. S.; Sui, Y; Ye, G-M.; Wang, H -y.; Liu, J-Q.; Wen-Tong. Synthesis, structures and
47 properties of three mercury coordination polymers based on 5-methyltetrazolate ligand. *J.*
48 *Solid State Chem.* **2018**, *263*, 182.

49
50 (70) Ohi, H.; Tachi, Y.; Itoh, S. Supramolecular and Coordination Polymer Complexes
51 Supported by a Tripodal Tripyridine Ligand Containing a 1,3,5-Triethylbenzene Spacer. *Inorg.*
52 *Chem.* **2004**, *43*, 4561-4563.

53
54 (71) Duriska, M. B.; Neville, S. M.; Batten, S. R. Variable length ligands: a new class of
55 bridging ligands for supramolecular chemistry and crystal engineering. *Chem. Commun.*
56 **2009**, 5579-5581.

1
2
3 (72) Adarsh, N. N.; Kumar, D. K.; Dastidar, P. Zn(II) metal–organic frameworks (MOFs)
4 derived from a bis-pyridyl-bis-urea ligand: effects of crystallization solvents on the structures
5 and anion binding properties. *CrystEngComm*. **2008**, *10*, 1565–1573.

6 (73) Adarsh, N. N.; Kumar, D. K.; Suresh, E.; Dastidar, P. Coordination polymers derived
7 from a bis-pyridyl-bis-amide ligand: Supramolecular structural diversities and anion binding
8 properties. *Inorg. Chim. Acta*. **2010**, *363*, 1367-1376.

9
10
11 (74) Lan, Y-Q.; Li, S -Li.; Qin, J-S.; Du, D-Y.; Wang, X-L.; Su, Z-M.; Fu, Q. Self-Assembly of
12 2D → 2D Interpenetrating Coordination Polymers Showing Polyrotaxane- and Polycatenane-
13 like Motifs: Influence of Various Ligands on Topological Structural Diversity. *Inorg. Chem*.
14 **2008**, *47*, 10600-10610.

15
16 (75) Ezuhara, T.; Endo, K.; Aoyama, Y. Helical Coordination Polymers from Achiral
17 Components in Crystals. Homochiral Crystallization, Homochiral Helix Winding in the Solid
18 State, and Chirality Control by Seeding. *J. Am. Chem. Soc.* **1999**, *121*, 3279-3283.

19
20 (76) Banerjee, S.; Adarsh, N. N.; Dastidar, P. An unprecedented all helical 3D network and a
21 rarely observed non-interpenetrated octahedral network in homochiral Cu(II) MOFs: effect of
22 steric bulk and π – π stacking interactions of the ligand backbone. *CrystEngComm*. **2009**,
23 *11*,746-749.

24
25 (77) Moon, S. Y.; Kim, E.; Noh, T. H.; Lee, Y. A.; Jung, O. S. Triple-meso helices as alcohol
26 reservoirs and discriminators: structural properties and thermal behaviors of silver(I)
27 coordination molecular braids containing diethylbis(4-pyridyl)silanes. *Dalton Trans.* **2013**, *42*,
28 13974-13980.

29
30 (78) Adarsh, N. N.; Dastidar, P. A Borromean Weave Coordination Polymer Sustained by
31 Urea–Sulfate Hydrogen Bonding and Its Selective Anion Separation Properties. *Cryst.*
32 *Growth Des.* **2010**, *10*, 483-487.

33
34 (79) Sekiya, R.; Nishikiori, S-i.; Kuroda, R. Combination between metal–ligand coordination
35 and hydrogen bond interaction: a facile route for the construction of 3D coordination
36 networks with the ability to include relatively large aromatic molecules. *CrystEngComm*.
37 **2009**, *11*, 2251-2253.

38
39 (80) Applegarth, L.; Goeta, A. E.; Steed, J. W. Influence of hydrogen bonding on coordination
40 polymer assembly. *Chem. Commun.* **2005**, 2405-2406.

41
42 (81) Hollmann, K.; Oppermann, A.; Witte, M.; Li, S.; Amen, M.; Flörke, U.; Egold, H.; Henkel,
43 G.; Herres-Pawlis, S. Copper(I) Complexes with Thiourea Derivatives as Ligands: Revealing
44 Secrets of Their Bonding Scheme. *Eur. J. Inorg. Chem.* **2017**, 1266–1279.

45
46 (82) Lu, H.; Zhu, Y.; Chen, N.; Gao, Y.; Guo, Y.; Li, G. Tang Ligand-Directed Assembly of a
47 Series of Complexes Bearing Thiourea-Based Carboxylates. *Cryst. Growth Des.* **2011**, *11*,
48 5241–5252.

49
50 (83) Succaw, G. L.; Weakley, T. J. R.; Han, F.; Doxsee, K. M. Crystal Engineering with
51 Bis(thiourea) Derivatives. *Cryst. Growth Des.* **2005**, *5*, 2288–2298.

52
53 (84) Custelcean, R. Crystal engineering with urea and thiourea hydrogen-bonding groups.
54 *Chem. Commun.* **2008**, 295-307.

1
2
3 (85) Wagner, J. P.; Schreiner, P. R. London Dispersion in Molecular Chemistry—
4 Reconsidering Steric Effects. *Angew. Chem. Int. Ed.* **2015**, *54*, 12274 – 12296.

5
6 (86) Liptrot, D. A.; Power, P. P. London dispersion forces in sterically crowded inorganic and
7 organometallic molecules. *Nat. Rev. Chem.* **2017**, *1*, 0004.

8
9 (87) Mitoraj, M. P.; Sagan, F.; Szczepanik, D. W.; de Lange, J. H.; Ptaszek, A. L.; van
10 Niekerk, D. M. E.; Cukrowski, I. Origin of Hydrocarbons Stability from a Computational
11 Perspective: A Case Study of Ortho-Xylene Isomers. *ChemPhysChem.* **2020**, *21*, 494–502.

12
13 (88) Cukrowski, I.; Sagan, F.; Mitoraj, M. P. On the Stability of Cis- and Trans-2-Butene
14 Isomers. An Insight Based on the FAMSEC, IQA, and ETS-NOCV Schemes. *J. Comput.*
15 *Chem.* **2016**, *37*, 2783-2798.

16
17 (89) Radi, S.; Youbi, Y.; Bacquet, M.; Degoutin, S.; Mabkhot, Y. N.; Garcia, Y. An
18 inorganic–organic hybrid material made of a silica-immobilized Schiff base receptor and its
19 preliminary use in heavy metal removal. *RSC Adv.* **2016**, *6*, 34212-34218.

20
21 (90) Sheldrick, G. M. SHELXS-97 and SHELXL-97, Program for Crystal Structure
22 Refinement; University of Gottingen: Germany. **1997**.

23
24 (91) Sheldrick, G. M. *Acta. Crystallogr.* **2008**, *A64*, 112.

25
26 (92) Kresse, G.; Furthmüller, J., Efficiency of ab-initio total energy calculations for metals and
27 semiconductors using a plane-wave basis set. *Comput. Mater. Sci.* **1996**, *6*, 15-50.

28
29 (93) Perdew, J. P.; Burke, K.; Ernzerhof, M., Generalized Gradient Approximation Made
30 Simple. *Phys. Rev. Lett.* **1996**, *77*, 3865-3868.

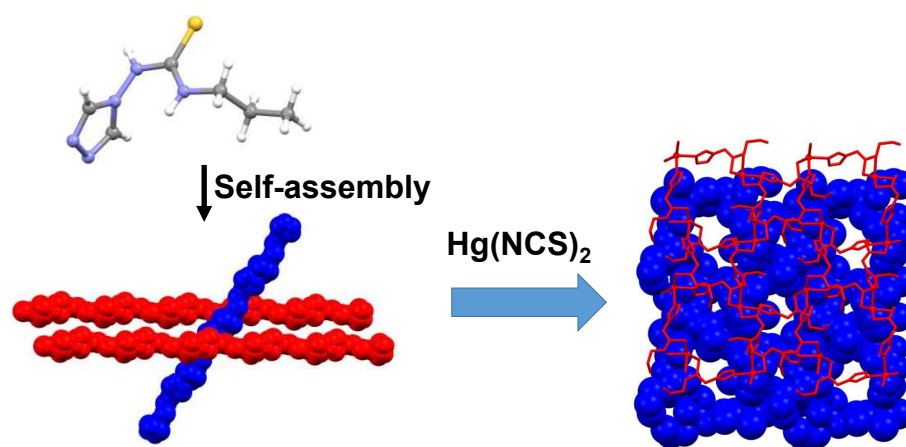
31
32 (94) Grimme, S.; Antony, J.; Ehrlich, S.; Krieg, H., A consistent and accurate ab initio
33 parametrization of density functional dispersion correction (DFT-D) for the 94 elements H-Pu.
34 *J. Chem. Phys.* **2010**, *132*, 154104.

35
36 (95) ADF2016, SCM, Theoretical Chemistry, Vrije Universiteit, Amsterdam, The Netherlands,
37 <http://www.scm.com>.

38
39 (96) te Velde, G.; Bickelhaupt, F. M.; Baerends, E. J.; Fonseca Guerra, C.; van Gisbergen,
40 S. J. A.; Snijders, J. G.; Ziegler, T., Chemistry with ADF. *J. Comput. Chem.* **2001**, *22*, 931-
41 967.
42
43
44
45
46
47
48
49
50
51
52
53
54
55
56
57
58
59
60

For Table of Contents Use Only**Exploring “triazole-thiourea” based Ligands for the Self-assembly of Photoluminescent Hg(II) Coordination Compounds**

Houria Benaissa,^a Nayarassery N. Adarsh,^b Koen Robeyns,^a Jakub J. Zakrzewski,^c Szymon Chorazy,^c James G. M. Hooper,^d Filip Sagan,^d Mariusz P. Mitoraj,^d Mariusz Wolff,^{a,e} Smaail Radi,^f Yann Garcia^{a,*}

TOC graphic**Synopsis**

This study represents the first explorative investigation on the supramolecular structural diversities in Hg coordination compounds having triazole-thiourea based ligands. Not less than seven crystal structures of such ligands and of 11 complexes, including coordination polymers are discussed. Their luminescence properties were studied and modeled by theoretical computations.

1
2
3
4
5
6
7
8
9
10
11
12
13
14
15
16
17
18
19
20
21
22
23
24
25
26
27
28
29
30
31
32
33
34
35
36
37
38
39
40
41
42
43
44
45
46
47
48
49
50
51
52
53
54
55
56
57
58
59
60